

Accepted Manuscript

Synthesis and anticancer activity of novel water soluble benzimidazole carbamates

Jae Eun Cheong, Michela Zaffagni, Ivy Chung, Yingjie Xu, Yiqiang Wang, Finith E. Jernigan, Bruce R. Zetter, Lijun Sun



PII: S0223-5234(17)30940-6

DOI: [10.1016/j.ejmech.2017.11.037](https://doi.org/10.1016/j.ejmech.2017.11.037)

Reference: EJMECH 9912

To appear in: *European Journal of Medicinal Chemistry*

Received Date: 9 August 2017

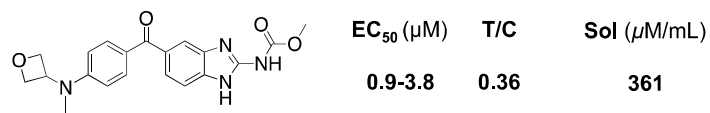
Revised Date: 6 November 2017

Accepted Date: 17 November 2017

Please cite this article as: J.E. Cheong, M. Zaffagni, I. Chung, Y. Xu, Y. Wang, F.E. Jernigan, B.R. Zetter, L. Sun, Synthesis and anticancer activity of novel water soluble benzimidazole carbamates, *European Journal of Medicinal Chemistry* (2018), doi: 10.1016/j.ejmech.2017.11.037.

This is a PDF file of an unedited manuscript that has been accepted for publication. As a service to our customers we are providing this early version of the manuscript. The manuscript will undergo copyediting, typesetting, and review of the resulting proof before it is published in its final form. Please note that during the production process errors may be discovered which could affect the content, and all legal disclaimers that apply to the journal pertain.

Graphic abstract



Synthesis and anticancer activity of novel water soluble benzimidazole carbamates

Authors:

Jae Eun Cheong^{#1}, Michela Zaffagni^{‡1}, Ivy Chung[^], Yingjie Xu[‡], Yiqiang Wang[#], Finith E. Jernigan[#], Bruce R. Zetter^{‡*}, Lijun Sun^{#*}

Affiliations:

[#]: Center for Drug Discovery and Translational Research, Beth Israel Deaconess Medical Center, Harvard Medical School, Boston, MA 02215, USA

[‡]: Vascular Biology Program, Boston Children's Hospital, Harvard Medical School, Boston, MA 02215, USA

[^] Department of Pharmacology, Faculty of Medicine, University of Malaya, Kuala Lumpur, Malaysia

*: Corresponding authors: bruce.zetter@childrens.harvard.edu (BZ), lsun1@bidmc.harvard.edu (LS)

¹ These authors contributed equally to this report.

Abstract

Metastases account for more than 90% of all cancer deaths and respond poorly to most therapies. There remains an urgent need for new therapeutic modalities for the treatment of advanced metastatic cancers. The benzimidazole methylcarbamate drugs, commonly used as anti-helminths, have been suggested to have anticancer activity, but progress has been stalled by their poor water solubility and poor suitability for systemic delivery to disseminated cancers. We synthesized and characterized the anticancer activity of novel benzimidazoles containing an oxetane or an amine group to enhance solubility. Among them, the novel oxetanyl substituted compound **18** demonstrated significant cytotoxicity toward a variety of cancer cell types including prostate, lung, and ovarian cancers with strong activity toward highly aggressive cancer lines (IC_{50} : 0.9-3.8 μ M). Compound **18** achieved aqueous solubility of 361 μ M. In a mouse xenograft model of a highly metastatic human prostate cancer, compound **18** (30 mg/kg) significantly inhibited the growth of established tumors (T/C: 0.36) without noticeable toxicity.

Key words: Anticancer activity; benzimidazole; solubility; oxetane

1. Introduction

Despite continued improvement in cancer therapy, there are few effective approaches for the treatment of metastatic cancers. Greater than 90% of all cancer deaths can be attributed to metastatic disease yet very few cancer drugs are developed through screens devoted to metastatic cancer. For many cancers, little progress has been made in extending the lives of patients with metastatic disease. It is estimated that in the US alone, 150,000 lung cancer patients and 26,000 prostate cancer patients will die from treatment-resistant metastasis in 2017. The molecular-targeted drugs are initially effective in treating metastatic lung cancers, but their benefit is limited by the rapid development of resistance and the improvement in lifespan is often still modest [1-4]. Further, the lack of efficacy of kinase inhibitor therapies in prostate cancer is likely due to the fact that activating tyrosine kinase mutations or amplifications are uncommon in castrate-resistant prostate cancer (CRPC) [5, 6]. Chemotherapies such as taxanes and androgen antagonists are effective in treating CRPC, but their benefit is limited by the emergence of treatment induced resistance. The development of safe and efficacious novel therapies that can overcome drug resistance holds great promise for metastatic cancer patients who are refractory to existing treatments.

Besides molecular targeted therapies that form the cornerstone of modern cancer precision medicine, repurposing of drugs used in other contexts has identified several novel approaches to cancer therapy, notably the use of thalidomide and its more recent analogs to treat multiple myeloma [7, 8]. The aggressiveness of late stage cancers is often driven by numerous orthogonal and compensatory signaling pathways that collectively promote metastatic tumor growth. The lack of a defined driver mutation renders many types of metastatic cancers as ‘undruggable’ via targeted therapies. Conversely, unbiased testing of approved drugs can reveal novel drug families

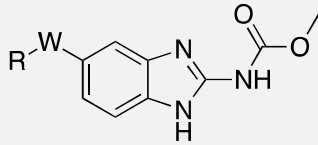
that can treat complex, metastatic cancers.

One important premise underlying drug repurposing is that the safety profile of approved drugs has been comprehensively characterized through many decades of clinical uses. Such efforts in drug repurposing have led to the identifications of anticancer effects by a number of commonly prescribed drugs [9]. The *in vitro* and *in vivo* anticancer activity of the broad spectrum anti-fungal drug itraconazole was demonstrated in medulloblastoma, glioblastoma, and non-small cell lung cancer (NSCLC) [10-12]. Another class of drugs that has emerged as potential anticancer agents is the anthelmintic benzimidazole drugs, which have been safely used for decades in the clinic for the treatment of gastrointestinal infections. The anthelmintic benzimidazole derivatives were found to exhibit potent inhibitory activity in brain tumor, colon cancer, breast cancer, leukemia, and myeloma [13-21]. One unique property of these benzimidazole drugs is their extremely low solubility that impedes their preclinical assessment via dosing regimens appropriate for clinical translation in the context of treatment of disseminated cancers. Herein we report our phenotypical screening approaches that identified the unique cytotoxicity profiles of the benzimidazoles in prostate cancer cell lines with high metastatic potentials as well as in lung cancer cells that are resistant to paclitaxel. We describe here, our novel structural modifications to improve the systemic anticancer activity of these compounds, the structure-activity relationship (SAR), and the discovery of a novel, water soluble oxetane-containing benzimidazole compound **18**, with potent anticancer activities in highly aggressive prostate, lung, and ovarian cancers.

2. Results and discussion

2.1. Cytotoxicity of anthelmintic benzimidazoles in aggressive prostate cancer cell lines

We first confirmed the *in vitro* anticancer activity of anthelmintic benzimidazole drugs using the prostate cancer cell line PC3M, a metastatic clone of the PC3 cell line, obtained by *in vivo* selection; and the PC3MLN4 cell line, an even more aggressive clone of PC3 obtained by recovering the cells from lymph nodes of mice after orthotopic injection into the mouse prostate (4 cycles) [22]. The original PC3 cell line was derived from bone metastasis of a prostate cancer and resistant to androgen depletion therapy [23, 24]. Compounds were analyzed for cytotoxicity after 48 hours (hr) drug treatment using Cyquant assay [25]. Our results confirmed the *in vitro* anticancer activity for several benzimidazoles, including albendazole, fenbendazole, flubendazole, and mebendazole) which, surprisingly, consistently demonstrated about two-fold higher anti-proliferative activity in the more highly aggressive PC3MLN4 cells (EC_{50} 0.6-0.9 μ M) than the less aggressive PC3M cells (EC_{50} 1.2-2.6 μ M) (**Table 1**). There seemed to be rather modest effect on the cytotoxicity by substituents (R-W) on the phenyl ring of the benzimidazole moiety. Thus, the EC_{50} of mebendazole and fenbendazole (which differ from each other by the linker -W- group), and that of mebendazole and flubendazole (which differ from each other by the addition of a fluoro group in the latter), is very similar in both the PC3MLN4 and the PC3M cancer cell lines. Even with more drastic changes in the chemical structures between albendazole (R: *n*-propyl) and fenbendazole (R: phenyl), the cytotoxicity of the two drugs does not differ much in both cell lines. We therefore reasoned that it would be plausible to achieve improvements in drug-like properties by modifying the R-W moiety without significantly compromising the anticancer activity of new benzimidazoles (*vide infra*).

Table 1. Cytotoxicity of anthelmintic benzimidazole in prostate cancer cell lines


Drug name	R	W	EC ₅₀ (μM)	
			PC3MLN4	PC3M
Flubendazole	4-Fluorophenyl	C=O	0.67	1.43
Albendazole	<i>n</i> -Propyl	S	0.58	1.15
Fenbendazole	Phenyl	S	0.91	2.60
Mebendazole	Phenyl	C=O	0.70	1.21

2.2. Drug design and chemistry

The benzimidazole anthelmintic drugs were originally developed for the topical treatment of parasitic infections in the gastrointestinal track. Because of their extremely poor aqueous solubility [26, 27] and low bioavailability [28-30], they are poorly suitable for systemic delivery in the setting of treating metastatic cancers. Increases in drug solubility can have a profound impact on drug pharmacokinetics/pharmacodynamics (PK/PD) and drug safety profiles [31, 32]. The solubility of organic molecules can be improved via incorporation of polar functional groups such as an amine. In addition, we were particularly interested in the 4-membered cyclic oxetane moiety, as it has been shown to dramatically increase water solubility and metabolic stability [33, 34]. We therefore pursued multiple structural modification strategies aimed to improve solubility and maintain anticancer activities of novel compounds containing the benzimidazole carbamate core. As outlined in **Figure 1**, one approach was to replace the methyl (CH₃) group of the

carbamate moiety with a solubility enhancing polar group (**A**); a second approach was to incorporate such a group on the phenyl moiety on the left-hand side of the molecule (**B**).

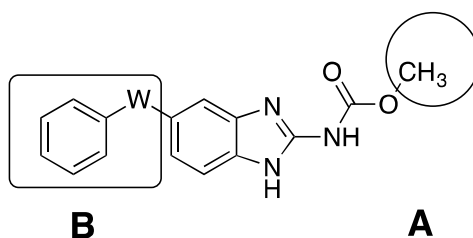
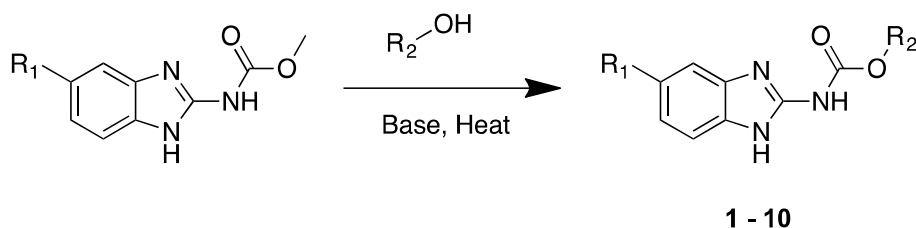


Figure 1. The right-hand side methyl group (highlighted by a circle) and the left-hand side moiety (highlighted by a rectangle) were modified to increase drug like properties. The linker W was determined by synthetic feasibility.

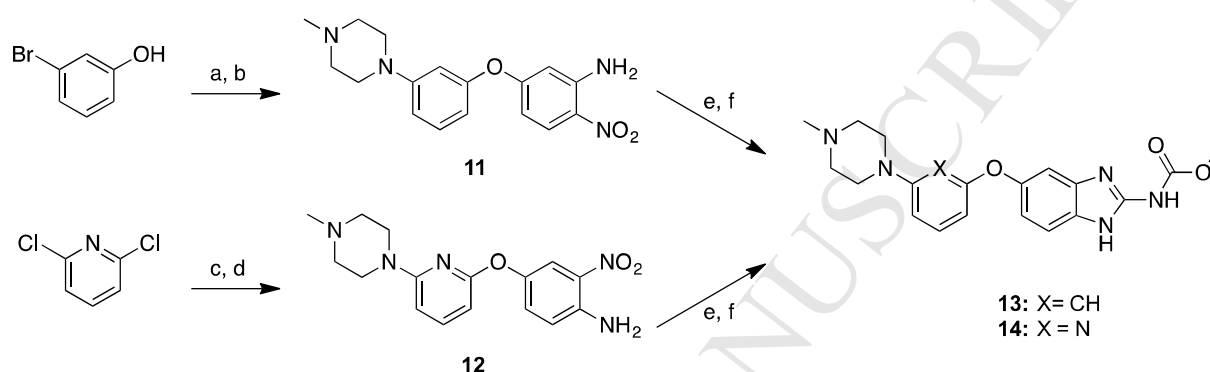
To pursue the approach **A**, a trans-esterification protocol was applied for the synthesis of new derivatives of the four active drugs albendazole, fenbendazole, flubendazole, and mebendazole where the right-hand side methylcarbamate was modified by incorporating a solubility enhancing moiety. The treatment of the benzimidazole methylcarbamates with an amino-ethanol, amino-propanol, or oxetanol in the presence of a base, resulted in the isolation of the desired products **1-10**, as crystalline solid after silica gel chromatographic purification (**Scheme 1**). The preparation of compounds **5** and **7** was facilitated by using microwave (MW) heating. Although the reaction was straightforward and successful in producing the desired products, the reaction condition was not optimized (yield: 10-30%) and confounded by the formation of the corresponding 2-aminobenzimidazole as a major side product.



Scheme 1. Conditions: **1** (R₁ = *n*-propylthio; R₂ = N,N-dimethylaminoethyl): pyridine, 100 °C, 3 hr; **2** (R₁ = *n*-propylthio; R₂ = N,N-dimethylaminopropyl): pyridine, 100 °C, 3 hr; **3** (R₁ = *n*-propylthio; R₂ = 3-oxetanyl): TEA, 90 °C, o/n; **4** (R₁ = *n*-propylthio; R₂ = (3-methyl-oxetan-3-yl)methyl): TEA, 90 °C, o/n; **5** (R₁ = benzoyl; R₂ = 3-oxetanyl): TEA/DMF, MW, 15 min; **6** (R₁ = 4-fluorobenzoyl; R₂ = N,N-dimethylaminopropyl): pyridine, 100 °C, 3 hr; **7** (R₁ = phenylthio; R₂ = 3-oxetanyl): TEA/DMF, MW, 15 min; **8** (R₁ = benzoyl; R₂ = N,N-dimethylaminoethyl): TEA/DMF, 110 °C, o/n; **9** (R₁ = 4-fluorobenzoyl; R₂ = N,N-dimethylaminoethyl): TEA/DMF, 110 °C, o/n; **10** (R₁ = phenylthio; R₂ = N,N-dimethylaminoethyl): TEA/DMF, 110 °C, o/n; TEA: triethylamine; DMF: N,N-dimethylformamide; o/n: overnight; hr: hour; min: minute; MW: microwave.

The modification of the left-hand side of the benzimidazole (approach **B**), by installing an amino or oxetanyl group, required *de novo* synthesis for each designed target molecule. We first synthesized new compounds containing an amino moiety aimed to improve solubility (**Scheme 2**). The intermediate compound **11** was prepared via a 2-step synthesis: palladium catalyzed amination [35] of 3-bromophenol with N-methylpiperazine was followed by nucleophilic substitution by 5-chloro-2-nitroaniline to install the ether linkage. The synthesis of intermediate compound **12** began with the nucleophilic substitution reaction between 4-amino-3-nitrophenol and 2,6-dichloropyridine to install the ether linkage, which was followed by the nucleophilic substitution reaction by N-methylpiperazine to incorporate the amino group. Next, the nitro group in intermediates **11** and **12** was reduced and the resulting 1,2-diamines were treated with 1,3-bis(methoxycarbonyl)-2-methyl-2-thiopseudourea to form the desired benzimidazoles **13** and **14** [36]. Our attempts to incorporate a carbonyl (-CO-) linker, instead of the ether (-O-) linker as

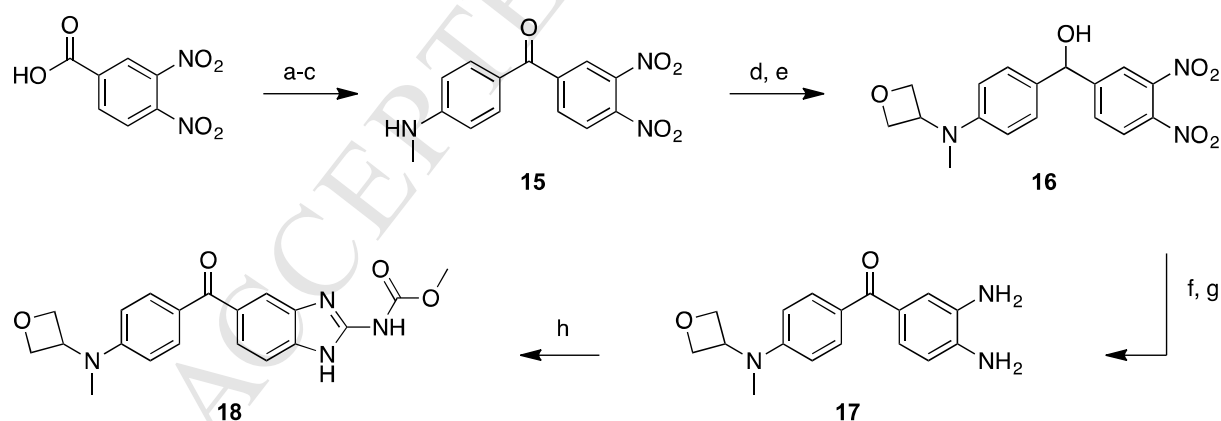
in compounds **13** and **14**, failed to yield the desired compounds due to decomposition during their multi-step syntheses. This strategy was not further pursued, because the oxetanyl derivatives afforded not only more potent anticancer activities but also dramatic improvement in aqueous solubility (*vide infra*).



Scheme 2. Conditions: (a) N-methylpiperazine, $\text{Pd}_2(\text{dba})_3$, *t*-BuONa, BINAP, toluene, 120 °C; (b) 5-chloro-2-nitroaniline, NaH, DMF, 120 °C; (c) 4-amino-3-nitrophenol, K_2CO_3 , DMF, 120 °C; (d) N-methylpiperazine, reflux; (e) zinc, AcOH; (f) 1,3-bis(methoxycarbonyl)-2-methyl-2-thiopseudourea, AcOH, 85 °C.

We next developed an eight-step synthetic procedure in order to incorporate an oxetane ring to the left-hand side of the benzimidazole scaffold (**Scheme 3**). The starting material 3,4-dinitrobenzoic acid was first converted to its acyl chloride and then carried forward for the Friedel-Crafts acylation of N-methylacetanilide. The syntheses were successfully scaled up to 600 mmol batch size and afforded the *para*- and *ortho*- regioisomers as a 4:1 mixture. After the acetyl protected amine was liberated by HCl mediated hydrolysis, the *para*-isomer **15** was isolated in 26% yield (overall from 3 steps). Attempts to install the oxetane moiety to intermediate **15** via reductive amination with 3-oxetanone were unsuccessful, likely due to the

weak basicity of the amine moiety (pK_a : 3.5) that was deactivated by the electron-withdrawing acyl group. We therefore reduced the ketone functional group in compound **15** to its corresponding alcohol, leading to increases of basicity of the amine (pK_a : 4.6), and then subjected it to reductive amination with 3-oxetanone to successfully generate the oxetane containing intermediate **16**. A 62% yield was obtained for the reductive amination step under microwave irradiation at 100 °C. The ketone functionality was next reinstated via Dess-Martin oxidation [37], and the nitro groups were reduced via palladium catalyzed hydrogenation to give the diamine intermediate **17** in 89% yield. The final product methyl (5-(4-(methyl(oxetan-3-yl)amino)benzoyl)-1H-benzo[d]imidazol-2-yl)carbamate (**18**) was obtained in 68% yield via microwave assistant condensation cyclization of 1,3-bis(methoxycarbonyl)-2-methyl-2-thiopseudourea and the intermediate **17**. Finally, the regioisomeric compound **19**, in which the oxetanyl moiety is *ortho* to the carbonyl group, was synthesized similarly from the *ortho*-isomer of intermediate **15**.



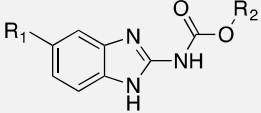
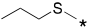
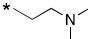
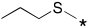
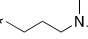
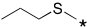
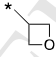
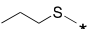

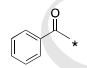
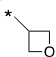
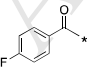
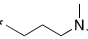
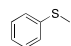
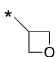
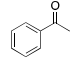
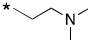
Scheme 3. Conditions: (a) $(\text{COCl})_2$, DCM, DMF (cat.), 0 °C to rt; (b) AlCl_3 , N-methylacetanilide, 100 °C; (c) HCl (conc.), H_2O ; (d) NaBH_4 , MeOH; (e) 3-oxetanone, AcOH, $\text{NaBH}_3(\text{CN})$, MeOH, MW, 30 W; (f) Dess-Martin periodinane, DCM; (g) Pd/C (10 wt %), H_2 , MeOH; (h) 1,3-bis(methoxycarbonyl)-2-methyl-2-thiopseudourea, MeOH, MW, 30 W.

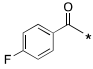
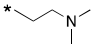
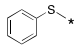
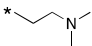
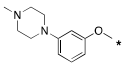
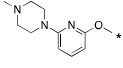
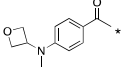
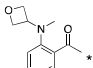
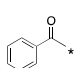
2.3. *In vitro* anticancer activities and structure-activity relationship (SAR)

The newly synthesized compounds were first evaluated for their cytotoxicity at 1 and 10 μ M concentrations in the non-small cell lung cancer (NSCLC) cell line A549, and the prostate cancer cell lines PC3 and PC3MLN4 (**Table 2**). Mebendazole, which we have confirmed to have anticancer activity in the PC3MLN4 cell line, was included as a reference compound for comparison. Cancer cells were treated with the compounds for 72 hr. Cell viability was measured by the MTT (3-(4,5-dimethylthiazol-2-yl)-2,5-diphenyltetrazolium bromide) assay, which is dependent upon the cellular metabolic activity of NAD(P)H flux. Compounds that inhibit the proliferation of rapidly dividing cancer cells will reduce the rates of MTT reduction. In at least two of the three cancer cell lines, the novel compounds **1**, **10**, **13**, **18**, and **19** induced significant cytotoxicity at 10 μ M concentration (cell viability: < 50%) while the other 9 compounds were much less active. Further, the compound **18**, a *para*-oxetanyl derivative of mebendazole, was the most potent compound and showed comparable activity to mebendazole at both 1 and 10 μ M concentrations in all three cell lines. In comparison, its *ortho*-oxetanyl isomer **19** showed significant cytotoxicity only at 10 μ M concentration. It is worth noting that modifications of the carbamate moiety lead to compounds (**1** - **10**) with reduced activity as compared with their parent methyl carbamates (e.g. mebendazole). Among them, only the N,N-dimethylaminoethyl derivative of albendazole (**1**) and that of fenbendazole (**10**) consistently showed cytotoxicity at 10 μ M, but not at 1 μ M concentration. The N,N-dimethylaminopropyl derivatives of albendazole (**2**) and flubendazole (**6**) did not show measurable cytotoxic activity. Importantly, and in contrast to compound **18**, incorporating an oxetane moiety onto the right-hand side of the benzimidazole resulted in compounds with diminished activity (**3** - **5**, **7**). Neither the N-methylpiperazine analogs

13 nor **14** were found highly active in the three cancer cell lines, although compound **13** showed activity at 10 μ M concentration. Taken together, our SAR results indicate that the benzimidazole molecules require the right-hand side methyl carbamate moiety to maintain high anticancer activity and are sensitive to modifications on the left-hand side of the structure. Significantly, incorporation of an oxetane moiety on the left-hand phenyl ring and *para* to the ketone functional group in mebendazole led to the observed high activity as demonstrated by compound **18**.

Table 2. Cytotoxicity of benzimidazole compounds at 1 and 10 μ M.

No.	R ₁	R ₂	<div style="text-align: center;">  </div>					
			% Viable Cells (\pm SD) ^a					
			PC3MLN4		PC3		A549	
			10 μ M	1 μ M	10 μ M	1 μ M	10 μ M	1 μ M
1			42.84 \pm 6.59	92.65 \pm 10.13	37.85 \pm 3.18	82.46 \pm 3.96	51.81 \pm 11.86	75.48 \pm 6.91
2			88.61 \pm 5.19	86.65 \pm 0.68	78.25 \pm 7.80	95.45 \pm 9.41	89.87 \pm 12.60	83.82 \pm 5.81
3			83.82 \pm 11.51	88.35 \pm 12.99	84.50 \pm 5.98	95.15 \pm 8.89	79.23 \pm 13.33	73.16 \pm 16.89
4			89.70 \pm 15.36	87.63 \pm 14.92	79.25 \pm 21.75	87.15 \pm 7.90	87.63 \pm 21.27	83.10 \pm 18.90
5			66.84 \pm 4.62	70.56 \pm 12.31	65.55 \pm 6.67	90.88 \pm 5.09	62.04 \pm 7.38	67.97 \pm 13.88
6			90.99 \pm 14.78	87.30 \pm 10.06	86.55 \pm 7.88	104.86 \pm 11.85	88.07 \pm 17.72	85.41 \pm 19.14
7			79.12 \pm 13.18	80.22 \pm 6.08	87.80 \pm 7.45	107.32 \pm 5.14	74.77 \pm 7.58	74.95 \pm 12.71
8			98.85 \pm 1.99	100.51 \pm 0.88	92.64 \pm 9.67	97.26 \pm 4.75	89.64 \pm 14.03	94.37 \pm 5.94

9			97.22 ± 3.89	84.62 ± 10.38	90.94 ± 3.13	91.21 ± 7.66	80.38 ± 12.33	89.41 ± 7.62
10			36.65 ± 1.76	98.11 ± 4.24	35.01 ± 5.31	88.86 ± 8.62	39.21 ± 6.89	91.81 ± 10.23
13		CH ₃	33.39 ± 3.01	86.33 ± 8.48	32.16 ± 3.27	73.11 ± 6.34	47.52 ± 12.38	76.96 ± 13.28
14		CH ₃	74.01 ± 8.85	82.97 ± 1.06	52.08 ± 14.68	98.14 ± 19.22	72.64 ± 7.22	87.85 ± 13.13
18		CH ₃	23.19 ± 4.54	34.94 ± 3.72	33.57 ± 1.82	44.50 ± 5.07	42.20 ± 5.46	50.19 ± 5.16
19		CH ₃	38.43 ± 2.42	100.44 ± 2.10	54.75 ± 5.12	100.67 ± 1.15	46.79 ± 9.23	98.98 ± 1.77
MBZ		CH ₃	24.94 ± 1.76	53.93 ± 6.44	35.77 ± 1.26	63.43 ± 9.84	50.77 ± 7.71	61.53 ± 6.57

^aData are average of three independent assays; SD: standard deviation; * indicates point for bond connection; MBZ: mebendazole.

We next conducted dose-response studies (3.2 nM - 50 μ M, five-fold serial dilutions) of the most active new benzimidazole compound **18** and determined its EC₅₀ in six cancer cell lines (Table 3). In the three lung cancer cell lines (H157, Calu1, and A549), compound **18** showed EC₅₀ ranging from 1.4 to 2.4 μ M. Consistent with the benzimidazole drugs (Table 1), compound **18** was highly cytotoxic to the aggressive PC3MLN4 prostate cancer cells (EC₅₀: 0.9 μ M), as well as the parent PC3 cells (EC₅₀: 1.6 μ M). Similar cytotoxic activity was observed for compound **18** in the SKOV3 ovarian cancer cells (EC₅₀: 1.0 μ M). Mebendazole, included as a positive reference compound in all assays, showed to be about twice as active as compound **18**; but the difference in activity between the two molecules lacks statistical significance (t-test).

Table 3. EC₅₀ of compound **18** in cancer cell viability assay

Cancer Type	Cell Line	EC ₅₀ ± SD (μM) ^a	
		18	Mebendazole
Lung	H157	2.4 ± 0.9	3.5 ± 1.4
	Calu1	1.6 ± 0.6	1.1 ± 0.3
	A549	1.4 ± 0.5	0.9 ± 0.1
Prostate	PC3	1.6 ± 0.6	1.1 ± 0.4
	PC3MLN4	0.9 ± 0.4	0.5 ± 0.2
Ovarian	SKOV3	1.0 ± 0.4	0.5 ± 0.1

^aData are average of three independent assays; SD: standard deviation.

Taxanes are standard care therapy for the treatment of metastatic prostate and lung cancers. However, cancers rapidly develop adaptive resistance and become refractory to taxanes. We asked if taxane-resistant cancer cells would still be sensitive to the treatment by compound **18**. We had shown previously that the anticancer activity of paclitaxel in the paclitaxel-resistant A549-TR cell line was > 100-fold less than in the parent A549 cells [38]. Encouragingly, we observed that both mebendazole and compound **18** reduced cell viability of the A549-TR cell line (**Figure 2**). As compared to the reduced sensitivity to paclitaxel (EC₅₀: 10.3 μM), both compound **18** (EC₅₀: 3.8 μM) and mebendazole (EC₅₀: 1.7 μM) were significantly more potent than paclitaxel alone (t-test, p-value < 0.05).

Taken together, these data suggest that the new benzimidazole compound **18** is a potent inhibitor of cancer cell growth, and that installation of the oxetane moiety in the left-hand side of mebendazole leads to little or no reduction in anticancer activity of compound **18** in most cell lines tested. If solubility is improved in this composition, it could lead to better promise for systemic *in vivo* delivery of the new drug for the treatment of disseminated tumors.

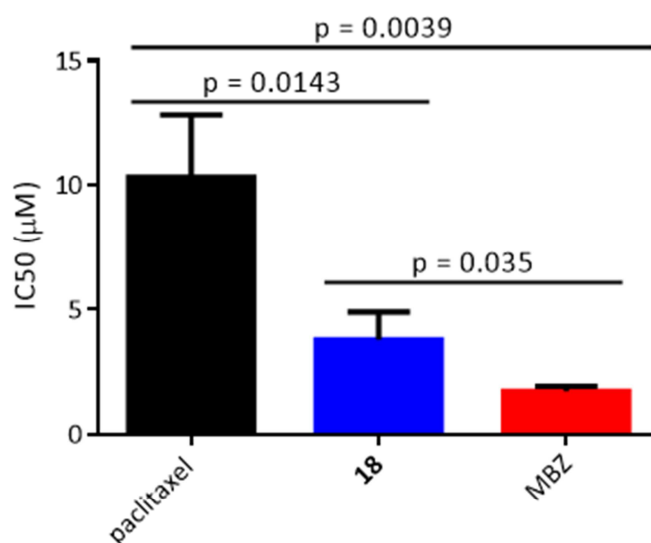


Figure 2. Anticancer activity of paclitaxel, compound **18**, and mebendazole (MBZ) in A549-TR. Data shown as the average \pm SD of three independent biological replicates. Statistical analysis was performed by t-test.

2.4. Cell cycle analyses

We conducted cell cycle analysis to determine the effects of compound **18** on cell cycle passage in PC3MLN4 prostate cancer cells (**Figure 3**). Cells were treated with compound **18** (1 μ M) or mebendazole (1 μ M), and the well characterized mitotic inhibitor nocodazole (1 μ M) was included as a positive control [39]. After 24 hr incubation, cells were harvested, fixed, stained with Propidium Iodide (PI) and finally counted by fluorescence-activated cell sorting (FACS) (**Figure 3A**). Collected data were analyzed with FlowJo software to determine the percentage of cells in G1, S, and G2 phase (**Figure 3B**) using the Dean/Jett/Fox Model [40]. Compound **18** caused accumulation of cells at the G2/M phase of the cell cycle. In contrast, mebendazole had a less significant effect on the accumulation of cells in G2/M. The cyclin B1 is a marker for cell cycle arrest at the G2/M phase. Indeed, compound **18**, as well as the positive control nocodazole,

increased cyclin B1 levels in cells after 24 hr treatment (**Figure 3C**). Taken together, these data suggest that compound **18** induces G2M cell cycle arrest.

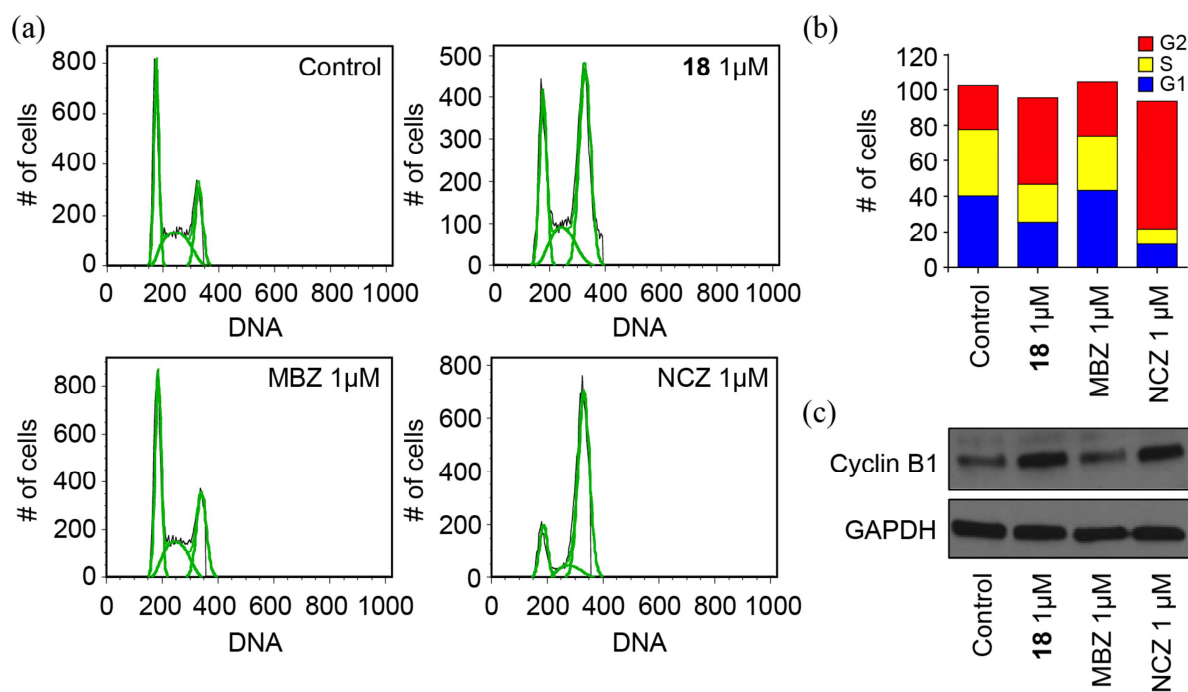


Figure 3. (a) Cell-cycle phase distribution of PC3MLN4 treated with compound **18**, mebendazole (MBZ) or nocodazole (NCZ) for 24 hr. Cell-cycle phase distribution was assessed by propidium iodide (PI) staining of permeabilized ethanol-fixed cells. (b) Graph reporting percentile cell-cycle phase distributions. G1-, S-, and G2-phase distributions were determined by FlowJo analysis. (c) Western blot showing an accumulation of Cyclin B1, expressed in G2 and M phase, in PC3MLN4 treated with compound **18**, MBZ, or NCZ for 24 hr.

2.5. Microtubule structures

The benzimidazole drugs similar to our lead compounds are known to disrupt microtubule structures [41-43], although other potential mechanisms have been suggested. These include blockade of hedgehog pathway signaling and interference with the action of the specific anti-apoptotic protein X-linked inhibitor of apoptosis (XIAP) [19, 44]. Microtubule structures perform vital cellular functions including intracellular organelle transportation, cell motion and

movement, as well as mitosis of proliferating cells. Therapeutic targeting of microtubule dynamics has led to the discovery and clinical success of the broadly used anticancer drugs taxanes, epothilones, and eribulin [45-47]. To determine whether compound **18** interfered with microtubule dynamics in cultured cancer cells, we incubated PC3MLN4 prostate cancer cells with compound **18** (1 μ M) for 48 hr and visualized microtubules by staining with anti-tubulin antibody (**Figure 4**). Our results demonstrate disruptions of the rearrangement and diminution of microtubules in cells treated with compound **18** to a degree similar to that of mebendazole (1 μ M) but less dramatic than nocodazole (1 μ M), a powerful but extremely toxic microtubule disruptor. This result indicates that compound **18** retains the activity of the parent compound in disrupting microtubule dynamics.

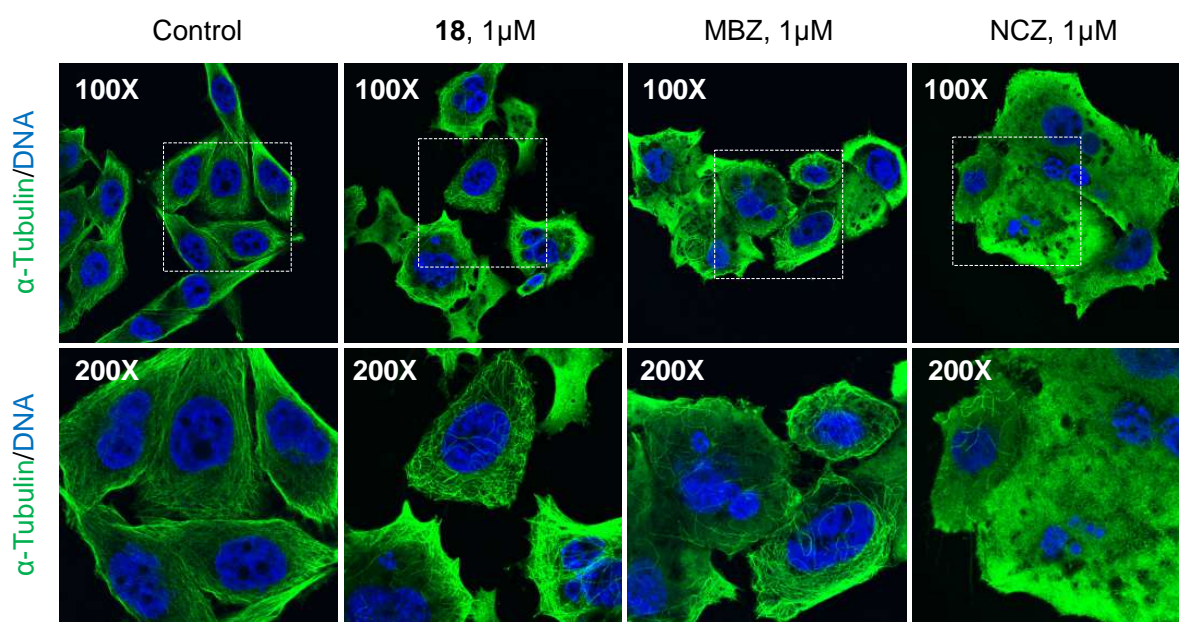


Figure 4. Representative immunofluorescence images showing the effect of compound **18**, mebendazole (MBZ), and nocodazole (NCZ) on microtubules in PC3MLN4 prostate cancer cells after treated for 48 hr. Dashed boxes in top row indicate area that are further magnified and shown in the bottom row. Tubulin structures are in green color; and DNA in blue.

2.6. Docking studies

The benzimidazole anthelmintic drugs are postulated to affect tubulin dynamics by their direct binding to the colchicine binding domain of tubulin [43]. We applied Autodock Vina [48] and performed docking study to model the interactions between compound **18** and tubulin utilizing the reported tubulin crystal structure (PDB Code: 3HKC) [49] (**Figure 5**). The simulation analyses suggest that the oxetanyl group of compound **18** participate in electrostatic interaction with Lys352, and together with the phenyl and benzimidazole moieties, occupy a hydrophobic packet composed of Leu248, Ala250, Leu255, Ala317, and Ile378. Neither the carbonyl group nor the amino group on the left-hand side of the molecule participated in H-bond interactions with the protein. Instead, they seem to optimally position the phenyl and the oxetanyl groups in the narrow hydrophobic packet. More importantly, the carbamate moiety forms hydrogen-bond (H-bond) interactions with Asn167, Tyr202, and Val238. It is likely that this network of H-bonds is required for the affinity of the benzimidazole compounds to the tubulin protein. This tight binding site can only accommodate small methyl group but not sterically bulky group such as oxetane, which might provide a rational to explain the significant loss of activity by compounds **1 - 10** (**Table 2**).

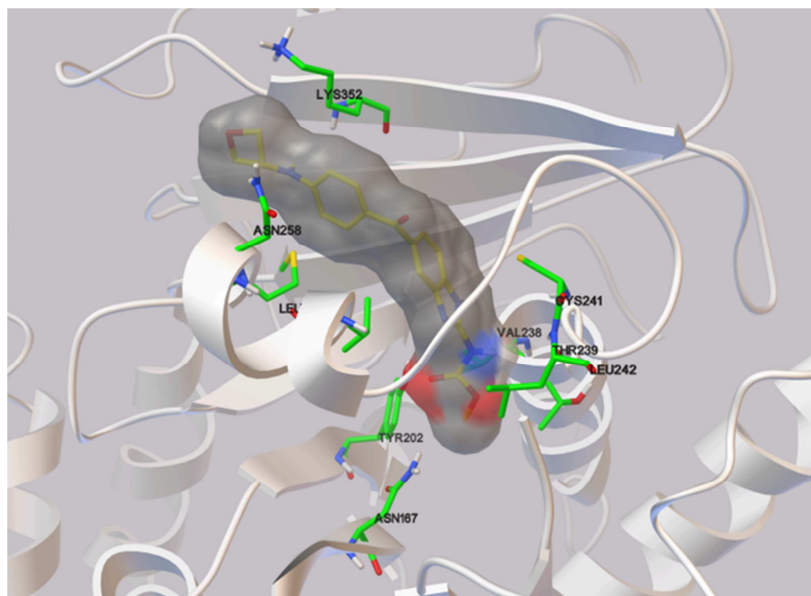


Figure 5. The lowest energy docking pose of **18** in the colchicine binding site of tubulin (PDB Code: 3HKC). Compound **18** is presented as yellow sticks and shaded in dark grey. Side chains of amino acids of tubulin protein involved in interactions with **18** are presented as green sticks. Nitrogen and oxygen atoms are colored as blue and red, respectively.

2.7. Solubility

Solubility is one most important physiochemical properties that dictates the performance of small molecule drugs. Drugs with low solubility often require the usage of toxic excipients to achieve adequate systemic delivery; and their absorption, hence therapeutic effects, is impaired by significant patient to patient variability [50-52]. In case of the benzimidazoles, as commonly used as anthelmintic drugs, they are at best only sparsely soluble in aqueous media. We compared the kinetic and thermodynamic solubility of mebendazole and the oxetanyl compound **18**. An HPLC method was developed to quantify the amount of solubilized mebendazole and compound **18**, respectively. The analytical method was optimized to achieve a detection limit of 1 µg/mL for both compounds. In pH 7.4 PBS buffer (**Table 4**), the kinetic (0.5 hr incubation)

and thermodynamic (24 hr incubation) solubility of mebendazole is below the 1 $\mu\text{g/mL}$ detection limit. Even after 120 hr incubation, there was still no measurable amount of mebendazole in solution. In contrast, the kinetic and thermodynamic solubility of compound **18** reached as high as 253 and 361 μM , respectively. Our data clearly indicates dramatic improvement of aqueous solubility by compound **18**, which could be attributed to the incorporation of the oxetanyl moiety in the molecule. Interestingly, the $\text{p}K_{\text{a}}$ of the nitrogen (N) atom that couples the oxetanyl group to the benzene ring is calculated as -0.51 (ChemAxon Version 14.8.18.0), indicative of a non-ionizable N atom. Therefore, the N linker is unlikely to contribute significantly to the enhanced solubility of compound **18**. Taken together, our results demonstrate the unique utility of oxetane for improving aqueous solubility as well as maintaining anticancer activity of mebendazole.

Table 4. Solubility of mebendazole and compound **18**

	Solubility ($\mu\text{g/mL}$) ^a	
	5% DMSO in PBS, pH 7.4	
	Mebendazole	18
30 min	< 1	96
24 hr	< 1	137

^a Solubility results are expressed as the mean of three independent measurements.

2.8. *In vivo* efficacy

We used the mouse PC3MLN4 xenograft tumor model to define the *in vivo* anticancer activity of systemically delivered compound **18** and compared the effect to mebendazole. PC3MLN4 cells (1×10^6 of cells) were injected subcutaneously between the scapular of nude

mice and allowed to grow to an average size of 35 mm³. Tumor-bearing mice were randomized and treated with compound **18** (30 mg/kg), mebendazole (30 mg/kg), and blank formulation (control group) via intraperitoneal (IP) injections (3 times a week for two weeks). Tumor volume and body weight (BW) were measured on the same days as the drug administrations as well as three days after the last dosing. As shown in **Figure 6A**, compound **18** and mebendazole showed statistically significant inhibition of tumor growth, and the effect of both drugs was very similar after day-9 of the study. This finding correlates well with the similar *in vitro* cytotoxicity of the two drugs in PC3MLN4 cells (**Table 3**). At the last measurement of the tumor volume (day-15), the mean (\pm SEM) size of the compound **18** treated group (T) is 43.2 mm³ (\pm 10.36) while that of the control group (C) is 118.8 mm³ (\pm 13.35) (**Figure 6C**). Therefore, the treatment-to-control (*T/C*) ratio for compound **18** at the last time point is 0.36 (t-test p value = 0.0481), below the *T/C* \leq 0.45 threshold that defines active antitumor activity [53]. The *T/C* for mebendazole is 0.31. The changes in body weight indicated that both drugs were well tolerated during the course of the treatment, although mebendazole induced a near 5% reduction in BW, and the changes were statistically significant on day-3 and day-5 (**Figure 6B**). This finding is consistent with reports by others that suggest the benzimidazole drugs could be safely dosed in preclinical models [19-21].

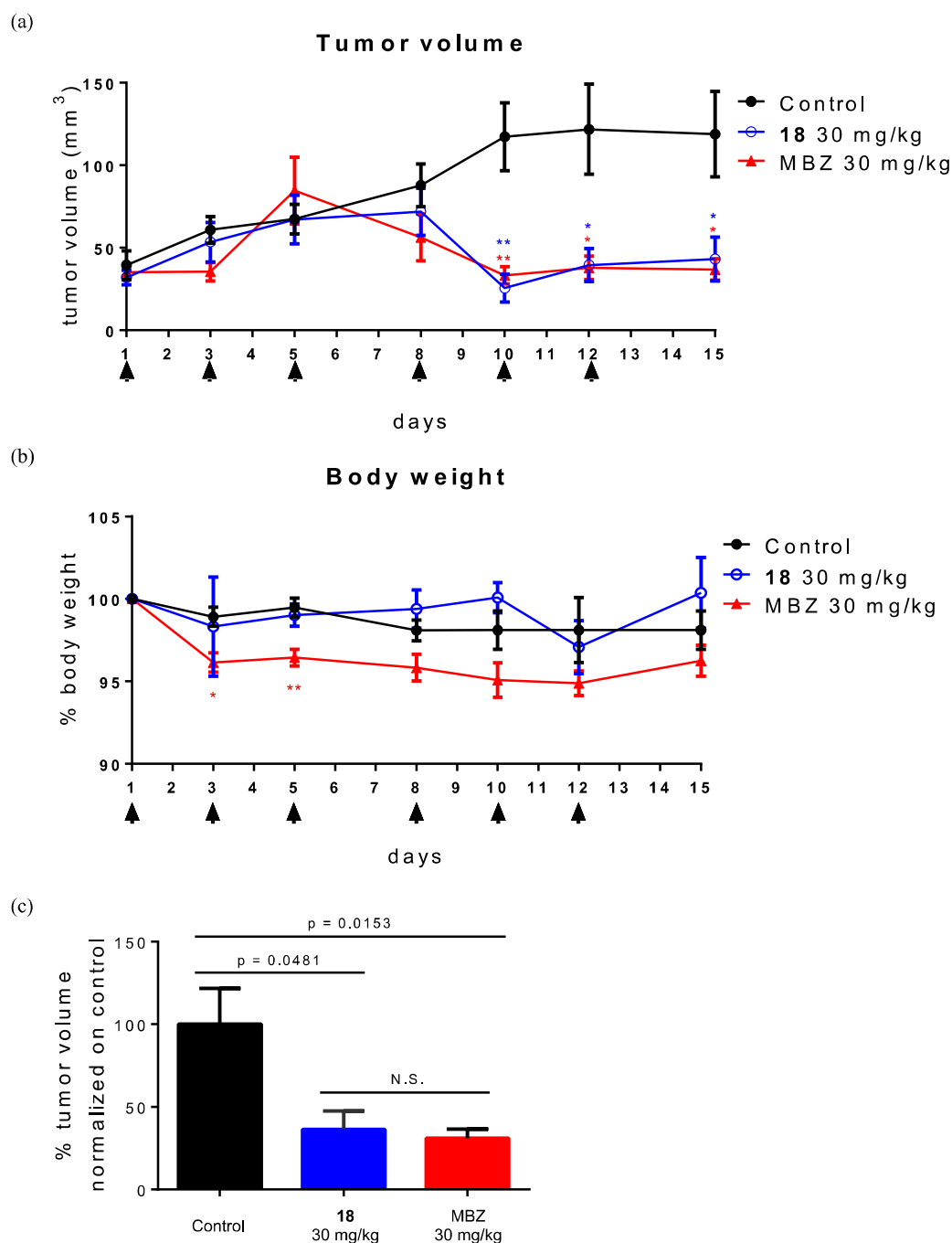


Figure 6. (a) Inhibition of tumor growth by compound **18** and mebendazole (MBZ) in PC3MLN4 xenograft tumor model; (b) the change in body weight, normalized as % of day-1 during the course of the study. Black arrows along the x-axis indicate dates of drug administration. Statistical analysis was performed by t-test. *: $p < 0.05$, **: $p < 0.01$.

Data shown as mean (\pm SEM). (c) Graph representing the % of tumor volume normalized on control on day 15. Data shown as mean (\pm SEM). Statistical analysis was performed by t-test. N.S.: not significant.

3. Conclusion

One promising strategy for the discovery of new and safe treatments for late stage progressive cancer is the rational design based on pre-clinical and clinical anticancer activities of existing drugs that are not prescribed for treating cancers. The benzimidazole anthelmintic drugs, including mebendazole, have been widely used in the clinic for decades to eliminate parasites in the gut. Their preclinical anticancer activities have been revealed recently. However, the clinical translation of those drugs for the treatment of cancer patients is impeded by the lack of adequate drug exposure [30]. Our results in this report provide intriguing findings that highly aggressive prostate cancer cells (PC3MLN4) and drug-resistant lung cancer cells (A549-TR) are highly vulnerable to the treatment by benzimidazoles. Furthermore, we succeeded in the design and synthesis of the novel lead compound **18** to dramatically improve aqueous solubility while maintaining potent anticancer activity in a range of cancer cells of the lung, prostate, and ovarian. In a mouse tumor xenograft model of the highly aggressive PCMLN4 prostate cancer, compound **18** significantly inhibited the tumor growth but showed no signs of toxicity. Similar to the benzimidazole drugs mebendazole and flubendazole, compound **18** induces cancer cell cycle arrest in the G2/M phase by disrupting tubulin dynamics. It is likely that aggressive cancer cells are more dependent on tubulin dynamics therefore are also more sensitive to the exposure to compound **18**. As part of our on-going research, we plan to delineate the mechanism of action and the molecular target of compound **18**. Although mebendazole gave equivalent anti-tumor effects when injected into animals via an intraperitoneal route, we hypothesize that this was due

to a depot effect where the drug remained in the peritoneum and slowly penetrated into the circulation. We expect that the improvement in aqueous solubility of compound **18** will enable sufficient systemic exposure to achieve therapeutic efficacy via oral administration, which would be problematic with the parent compounds. We will report in due course the detailed characterizations of compound **18** in *in vitro* and *in vivo* pharmacokinetics and pharmacodynamics.

4. Experimental Section

4.1. Chemistry

4.1.1. General

All reagents and solvents were purchased from commercially available sources and used without further purification. All reactions were carried out according to the indicated procedures and conditions. Flash Chromatography was performed on an Interchim PuriFlash 430 with cartridges filled with Silica gel 50 μm (PF-50SIHC). Reactions were monitored by LC/MS analysis and/or thin-layer chromatography (TLC) on silica-coated glass with the indicated eluent. The compounds were visualized by UV light (254 nm). LC/MS analysis was performed on an Agilent 1200 HPLC/UV ($\lambda = 220$ nm and/or 254 nm) system coupled with a mass spectroscopic (Applied Biosystems, MDS SCIEX, Q TRAP LC/MS/MS) detector. High-resolution mass spectrometry (HRMS) was performed on a Waters Q-TOF PremierTM Mass Spectrometer in the positive mode that utilizes electrospray ionization (ESI). Compounds for analysis were dissolved in 100% DMSO and separated on C18 cartridge (particle size 2.6 μm , dimensions: 100 mm X 2.1 mm, 0.3 mL/min flow rate, 1 μL injection volume) using acetonitrile/water mobile phase

with 0.1% formic acid as a modifier. The gradient started at 0% acetonitrile, held for 1 min, and linearly increased to 97% acetonitrile over 10 min, with 2 min hold at 97% acetonitrile and subsequent re-equilibration to the original conditions in a total of 17 min. All compounds reported were obtained in a purity of > 95% at 254 nm wavelength. Nuclear magnetic resonance (^1H NMR) spectra were recorded on a Varian Mercury plus NMR spectrometer operating at 400.13 MHz frequencies for ^1H , using a 5 mm ASW PFG probe capable of detecting ^1H and ^{13}C nuclei. The proton chemical shifts (ppm) were referenced to the tetramethylsilane (TMS) internal standard (0 ppm). Chemical shifts (δ) are reported related to CDCl_3 or $\text{DMSO}-d_6$ residual solvent peaks and indicated in parts per million (ppm). The splitting patterns are abbreviated as follows: s (singlet), d (doublet), dd (doublet of doublets), t (triplet), q (quartet), quin (quintet), sxt (sextet), triplet of doublets (td), br (broad), and m (multiplet).

General Procedure to Synthesis of Bendazole Moiety with Different Side Chains (Compounds 1 - 10)

To a stirred mixture of each bendazole in base/solvent (100 mM) were added 10 equiv of alcohols indicated in **Scheme 1**. The reaction proceeded at 90, 100, or 110 °C for 3 hr to o/n. For compounds **5** and **7**, the reaction mixture was exposed to microwave irradiation for 5 - 15 min at 60 or 70 °C. Workup: Once the reaction was complete, the solvent was removed under reduced pressure, diluted with four times the reaction volume of EtOAc and washed with water and brine. The organic layer was dried with Na_2SO_4 and concentrated in vacuo, followed by purification performed on automated flash chromatography system with the desired method commented below.

2-(Dimethylamino)ethyl (5-(propylthio)-1H-benzo[d]imidazol-2-yl)carbamate (1)

Isolated by silica gel chromatography with DCM:MeOH = 3:1 as an off-white solid; R_f = 0.32 (10% MeOH/DCM); HPLC analysis (C18 reverse phase, 17 mins, 0-97% H₂O/ACN with 0.1% formic acid): t_R = 7.6 min; ¹H NMR (400 MHz, 25 °C, CDCl₃) δ 7.57 (1H, br), 7.45 (1H, br), 7.25 (1H, d, J = 8.2 Hz), 4.45, (2H, t, J = 6.1 Hz), 2.88 (2H, t, J = 7.2 Hz), 2.79 (2H, t, J = 6.1 Hz), 2.37 (6H, s), 1.64 (2H, sxt, J = 7.4 Hz), 1.01 (3H, t, J = 7.2 Hz); MS (ESI) m/z : [M + H]⁺ Calcd for C₁₅H₂₃N₄O₂S 323.2; Found 323.6.

3-(Dimethylamino)propyl (5-(propylthio)-1H-benzo[d]imidazol-2-yl)carbamate (2)

Isolated by silica gel chromatography with DCM:MeOH = 3:1 as an off-white solid; R_f = 0.07 (10% MeOH/DCM); HPLC analysis (C18 reverse phase, 17 mins, 0-97% H₂O/ACN with 0.1% formic acid): t_R = 7.6 min; ¹H NMR (400 MHz, 25 °C, CDCl₃) δ 7.59 (1H, br), 7.42 (1H, br), 7.26 (1H, d, J = 7.8 Hz), 4.43 (2H, t, J = 6.7 Hz), 2.87 (2H, t, J = 7.2 Hz), 2.47 (2H, t, J = 6.8 Hz), 2.26 (6H, s), 2.04 (2H, quin, J = 6.8 Hz), 1.64 (2H, sxt, J = 7.3 Hz), 1.01 (3H, t, J = 7.4 Hz); MS (ESI) m/z : [M + H]⁺ Calcd for C₁₆H₂₅N₄O₂S 337.2; Found 337.6.

Oxetan-3-yl (5-(propylthio)-1H-benzo[d]imidazol-2-yl)carbamate (3)

Isolated by silica gel chromatography with DCM:MeOH = 40:1 as a white solid; R_f = 0.38 (10% MeOH/DCM); HPLC analysis (C18 reverse phase, 17 mins, 0-97% H₂O/ACN with 0.1% formic acid): t_R = 9.2 min; ¹H NMR (400 MHz, 25 °C, CDCl₃) δ 12.02 (1H, br), 7.50 (1H, s), 7.41 (1H, d, J = 8.2 Hz), 7.13 (1H, d, J = 8.6 Hz), 5.28 (1H, br), 4.88-4.84 (1H, m), 4.32 (1H, t, J = 9.4 Hz), 4.02 (1H, dd, J = 9.4, 5.9 Hz), 3.75-3.60 (2H, m), 2.86 (2H, t, J = 7.2 Hz), 1.54 (2H, sxt, J = 7.2 Hz), 0.94 (3H, t, J = 7.2 Hz); MS (ESI) m/z : [M + H]⁺ Calcd for C₁₄H₁₈N₃O₃S 308.1; Found 308.6.

(3-Methyloxetan-3-yl)methyl (5-(propylthio)-1H-benzo[d]imidazol-2-yl)carbamate (4)

Isolated by silica gel chromatography with hexanes:EtOAc = 1:1 as a white solid; R_f = 0.41 (10% MeOH/DCM); HPLC analysis (C18 reverse phase, 17 mins, 0-97% H₂O/ACN with 0.1% formic acid): t_R = 9.1 min; ¹H NMR (400 MHz, 25 °C, CDCl₃) δ 7.52 (1H, br), 7.36 (1H, br), 7.25 (1H, d, J = 7.9 Hz), 4.62 (2H, d, J = 6.3 Hz), 4.54 (2H, d, J = 5.9 Hz), 4.50 (2H, s), 2.88 (2H, t, J = 7.4 Hz), 1.64 (2H, sxt, J = 7.4 Hz), 1.40 (3H, s), 1.01 (3H, t, J = 7.4 Hz); MS (ESI) m/z : [M + H]⁺ Calcd for C₁₆H₂₂N₃O₃S 336.1; Found 336.5.

Oxetan-3-yl (5-benzoyl-1H-benzo[d]imidazol-2-yl)carbamate (5)

Isolated by silica gel chromatography with DCM:MeOH = 3:1 as a white solid; R_f = 0.56 (10% MeOH/DCM); white solid (180 mg, 53%); HPLC analysis (C18 reverse phase, 17 mins, 0-97% H₂O/ACN with 0.1% formic acid): t_R = 8.7 min; ¹H NMR (400 MHz, 25 °C, CDCl₃) δ 12.42-12.31 (1H, m), 7.95-7.54 (8H, m), 5.27 (1H, t, 5.7), 4.92-4.85 (1H, m), 4.30-4.24 (1H, m), 4.08-4.02 (1H, m), 3.76-3.72 (1H, m), 3.65-3.61 (1H, m); MS (ESI) m/z : [M + H]⁺ Calcd for C₁₈H₁₆N₃O₄ 338.1; Found 338.5.

3-(Dimethylamino)propyl (5-(4-fluorobenzoyl)-1H-benzo[d]imidazol-2-yl)carbamate (6)

Isolated by silica gel chromatography with DCM:MeOH = 2:1 as an off-white solid; R_f = 0.08 (10% MeOH/DCM); HPLC analysis (C18 reverse phase, 17 mins, 0-97% H₂O/ACN with 0.1% formic acid): t_R = 7.9 min; ¹H NMR (400 MHz, 25 °C, DMSO-*d*₆) δ 7.84 (1H, s), 7.80 (2H, dd, J = 8.2, 5.9 Hz), 7.56-7.51 (2H, m), 7.38 (2H, t, J = 8.6 Hz), 4.23 (2H, t, J = 6.5 Hz), 2.57 (2H, t, J = 6.8 Hz), 2.33 (6H, s), 1.88 (2H, quin, J = 6.8 Hz); MS (ESI) m/z : [M + H]⁺ Calcd for

$C_{20}H_{22}FN_4O_3$; Found 385.2; Found 385.6.

Oxetan-3-yl (5-(phenylthio)-1H-benzo[d]imidazol-2-yl)carbamate (7)

Isolated by silica gel chromatography with DCM:MeOH = 9:1 as a yellow solid; R_f = 0.49 (10% MeOH/DCM); HPLC analysis (C18 reverse phase, 17 mins, 0-97% H_2O /ACN with 0.1% formic acid): t_R = 9.5 min; 1H NMR (400 MHz, 25 °C, $CDCl_3$) δ 12.22-12.13 (1H, m), 7.58 (1H, d, 6.3), 7.52 (1H, t, J = 7.6 Hz), 7.31-7.11 (6H, m), 5.27 (1H, t, J = 5.5 Hz), 4.87 (1H, d, J = 3.5 Hz), 4.24 (1H, td, J = 9.3, 4.5 Hz), 4.05-4.00 (1H, m), 3.76-3.59 (2H, m); MS (ESI) m/z : $[M + H]^+$ Calcd for $C_{17}H_{16}N_3O_3S$ 342.1; Found 342.4.

2-(Dimethylamino)ethyl (5-benzoyl-1H-benzo[d]imidazol-2-yl)carbamate (8)

Isolated by silica gel chromatography with DCM:MeOH = 9:1 as a white solid; R_f = 0.21 (10% MeOH/DCM); HPLC analysis (C18 reverse phase, 17 mins, 0-97% H_2O /ACN with 0.1% formic acid): t_R = 7.9 min; 1H NMR (400 MHz, 25 °C, $DMSO-d_6$) δ 7.86 (1H, s), 7.72 (2H, d, J = 7.8 Hz), 7.67-7.63 (1H, m), 7.59-7.52 (4H, m), 4.28 (2H, t, J = 5.6 Hz), 2.55 (2H, t, J = 5.6 Hz), 2.20 (6H, s); MS (ESI) m/z : $[M + H]^+$ Calcd for $C_{19}H_{21}N_4O_3$ 353.2; Found 353.6.

2-(Dimethylamino)ethyl (5-(4-fluorobenzoyl)-1H-benzo[d]imidazol-2-yl)carbamate (9)

Isolated by silica gel chromatography with DCM:MeOH = 9:1 as a white solid; R_f = 0.24 (10% MeOH/DCM); HPLC analysis (C18 reverse phase, 17 mins, 0-97% H_2O /ACN with 0.1% formic acid): t_R = 8.1 min; 1H NMR (400 MHz, 25 °C, $DMSO-d_6$) δ 7.84 (1H, s), 7.80 (2H, dd, J = 8.1, 5.6 Hz), 7.56-7.51 (2H, m), 7.38 (2H, t, J = 8.8 Hz), 4.28 (2H, t, J = 5.6 Hz), 2.55 (2H, t, J = 5.6 Hz), 2.20 (6H, s); MS (ESI) m/z : $[M + H]^+$ Calcd for $C_{19}H_{20}FN_4O_3$ 371.2; Found 371.5.

2-(Dimethylamino)ethyl (5-(phenylthio)-1H-benzo[d]imidazol-2-yl)carbamate (10)

Isolated by silica gel chromatography with DCM:MeOH = 9:1 as a white solid; R_f = 0.26 (10% MeOH/DCM); HPLC analysis (C18 reverse phase, 17 mins, 0-97% H₂O/ACN with 0.1% formic acid): t_R = 8.6 min; ¹H NMR (400 MHz, 25 °C, DMSO-*d*₆) δ 7.53 (1H, s), 7.46 (1H, d, J = 8.3 Hz), 7.27 (2H, t, J = 7.4 Hz), 7.20-7.16 (2H, m), 7.12 (2H, d, J = 7.8 Hz), 4.27 (2H, t, J = 5.6 Hz), 2.56 (2H, t, J = 5.6 Hz), 2.20 (6H, s); MS (ESI) m/z : [M + H]⁺ Calcd for C₁₈H₂₁N₄O₂S 357.1; Found 357.4.

Methyl (5-((6-(4-methylpiperazin-1-yl)pyridin-2-yl)oxy)-1H-benzo[d]imidazol-2-yl)carbamate 5-(3-(4-Methylpiperazin-1-yl)phenoxy)-2-nitroaniline (11)

To a stirred solution of 3-bromophenol (0.6 g, 3.5 mmol) in anhydrous toluene (12 mL) was added N-methylpiperazine (0.5 mL, 4.2 mmol), Pd₂(dba)₃ (79 mg, 0.087 mmol), ^tBuONa (0.933 g, 9.7 mmol), and BINAP (0.216 g, 0.35 mmol) in this sequence. The resulting solution was heated to reflux under argon for 1 hr. Upon completion (monitored by LC/MS), the mixture was cooled to rt, extracted with EtOAc and brine, dried over Na₂SO₄, and concentrated under reduced pressure to give the crude product. Purification was performed on an automated flash chromatography system with 0-10% MeOH in DCM to yield 0.38 g (56%). To a biaryl ether intermediate (0.360 mg, 1.87 mmol) in anhydrous DMF (1.5 mL) was added 60% NaH (189 mg) slowly, followed by 5-chloro-2-nitroaniline (1.29 g, 7.48 mmol) under argon. The resulting mixture was stirred overnight at 120 °C. Once the reaction was complete, the mixture was cooled to rt and ice water was added. The product was extracted with EtOAc, washed with brine, dried over Na₂SO₄, and concentrated under reduced pressure. Purification was performed on an

automated flash chromatography system with 0-10% MeOH in DCM to afford 0.41 g (66%) of the product **11**.

4-((6-(4-Methylpiperazin-1-yl)pyridin-2-yl)oxy)-2-nitroaniline (12)

To a stirred solution of 2,6-dichloropyridine (0.48 g, 3.24 mmol) and 4-amino-3-nitrophenol (0.5 g, 3.24 mmol) in anhydrous DMF (15 ml) was added potassium carbonate (0.67 g, 4.87 mmol) under argon. The resulting mixture was stirred overnight at 120 °C. Upon completion (monitored by LC/MS), the mixture was cooled to rt, extracted with EtOAc and brine, dried over Na₂SO₄, and concentrated under reduced pressure to give the desired product (750 mg, 87%). Biaryl ether intermediate (0.44 g, 1.5 mmol) was dissolved in 8.8 mL of N-methylpiperazine and the resulting solution was refluxed for 3 hr. Once the reaction was complete, the mixture was cooled to rt and ice water was added. The product was extracted with EtOAc, washed with brine, dried over Na₂SO₄, and concentrated under reduced pressure to give **12** for the next step without purification.

Methyl (5-(3-(4-methylpiperazin-1-yl)phenoxy)-1H-benzo[d]imidazol-2-yl)carbamate (13)

Compound **11** (0.30 g, 0.90 mmol) was treated with zinc dust (0.41 g, 6.3 mmol) in acetic acid (19 mL) for 1 hr at rt. The mixture was filtered through Celite and the filter cake was washed with DCM. The filtrate was then concentrated under reduced pressure. The pH was adjusted to ~8 by the dropwise addition of 5 M NaOH and DCM was added to product crashing out of solution. The precipitate was isolated by vacuum filtration and dried under high vacuum to yield 151 mg (42%). To a stirred solution of diaminoaryl intermediate (0.14 g, 0.46 mmol) in acetic acid (4 mL) was added 1,3-bis(methoxycarbonyl)-2-methyl-2-thiopseudourea (0.24 g, 1.2 mmol) under argon. The resulting solution was stirred at 85 °C for 1 hr. Upon completion

(monitored by LC/MS), the mixture was cooled to rt, the solvent was removed under reduced pressure. 2M HCl (9 mL) was added to the residue and the mixture was stirred at r.t. for 1 hr. The product was extracted with EtOAc and brine, dried over Na₂SO₄, and concentrated under reduced pressure to give the crude product. Purification was performed on an automated flash chromatography system with 0-10% MeOH in DCM to yield 74 mg (42%) of **13** as a pale yellow solid. HPLC analysis (C18 reverse phase, 17 mins, 0-97% H₂O/ACN with 0.1% formic acid): t_R = 7.3 min; ¹H NMR (400 MHz, 25 °C, CD₃OD) δ 11.65 (2H, br), 7.38 (1H, d, J = 8.2 Hz), 7.13 (1H, t, J = 8.2 Hz), 7.03 (1H, s), 6.79 (1H, d, J = 8.6 Hz), 6.64 (1H, d, J = 8.6 Hz), 6.53 (1H, s), 6.78 (1H, d, J = 7.8 Hz), 3.74 (3H, s), 3.09 (4H, s), 2.40 (4H, s), 2.19 (3H, s); MS (ESI) m/z : [M + H]⁺ Calcd for C₂₀H₂₄N₅O₃ 382.1874; Found 382.1878.

Methyl (5-((6-(4-methylpiperazin-1-yl)pyridin-2-yl)oxy)-1H-benzo[d]imidazol-2-yl)carbamate (14)

The substrate **12** (595 mg, 1.8 mmol) was treated with zinc dust (827 mg, 12.6 mmol) in acetic acid (39 ml) for 10 hr at rt. The mixture was filtered through Celite and the filter cake was washed with EtOAc. The filtrate was then concentrated under reduced pressure. The pH was adjusted to ~8 by the dropwise addition of 5 M NaOH and EtOAc was added to crash the product out of solution. The precipitate was isolated by vacuum filtration and dried under high vacuum to yield 395 mg (72%). To a stirred solution of diaminoaryl intermediate (290 mg, 0.97 mmol) in acetic acid (8 mL) was added 1,3-bis(methoxycarbonyl)-2-methyl-2-thiopseudourea (499 mg, 2.42 mmol) under argon. The resulting solution was stirred for 1 hr at 85 °C. Upon completion (monitored by LC/MS), the mixture was cooled to rt, and the solvent was removed under reduced pressure. 2M HCl (15 mL) was added to the residue and the mixture was stirred at r.t. for 1 hr. The product was extracted with EtOAc and brine, dried over Na₂SO₄, and concentrated

under reduced pressure to give the crude product. Purification was performed on an automated flash chromatography system with 0-10% MeOH in DCM to yield 94 mg (25%) of **14** as a pale yellow solid. HPLC analysis (C18 reverse phase, 17 mins, 0-97% H₂O/ACN with 0.1% formic acid): t_R = 7.1 min; ¹H NMR (400 MHz, 25 °C, CD₃OD) δ 11.65 (2H, s), 7.49 (1H, t, J = 8.0 Hz), 7.38 (1H, d, J = 8.6 Hz), 7.13 (1H, s), 6.83 (1H, d, J = 8.2 Hz), 6.43 (1H, d, J = 8.2 Hz), 6.01 (1H, d, J = 7.8 Hz), 3.75 (3H, s), 3.33 (4H, s), 2.30 (4H, s), 2.16 (3H, s); MS (ESI+) C₁₉H₂₂N₆O₃ m/z Calcd for (M+H)⁺ 383.2; Found 383.2.

(3,4-Dinitrophenyl)(4-(methylamino)phenyl)methanone (15)

3,4-Dinitrobenzoic acid (127 g, 600 mmol) was suspended in DCM (200 mL) and oxalyl chloride (154 mL, 1.8 mole) was added slowly. The reaction mixture was then cooled in an ice bath, and DMF (2 mL) was added dropwise over 2 hr. The resulting mixture was stirred for 3 hr at 0 °C and for 1 hr at rt (or until the solution become transparent at rt). Upon completion (monitored by LC/MS), the solution was concentrated under reduced pressure and residual oil was placed under the high vacuum pump for 30 min to remove the residual amount of oxalyl chloride. To this dark yellow viscous oil, AlCl₃ (296 g, 2.2 mole) was added in small portion over 15 min* with a gentle swirl by hands and followed by the addition of N-methyl-N-phenylacetamide (150 g, 1.0 mole) was added. The resulting mixture was stirred at 100 °C for overnight. Once the reaction was complete, the excess AlCl₃ was quenched by the slow addition of water (100 mL) and extracted with DCM, dried over Na₂SO₄, and concentrated to yield an amber, viscous oil. Purification was performed on automated flash chromatography system with 0-100% EtOAc in hexanes. The product elutes at ~40% EtOAc to afford 47% yield of *ortho*- and *para*- mixture.** R_f = 0.58 (10% MeOH/DCM); HPLC analysis (C18 reverse

phase, 17 mins, 0-97% H₂O/ACN with 0.1% formic acid): t_R = 9.9 min; ¹H NMR (400 MHz, 25 °C, CDCl₃) δ 8.33 (s, 1H), 8.17 (m, 1H), 8.05 (d, 1H), 7.85 (d, 2H), 7.42 (d, 2H), 3.35 (s, 3H), 2.05 (s, 3H); MS (ESI) m/z : [M + H]⁺ Calcd for C₁₆H₁₄N₃O₆ 344.1; Found 344.2. *Note: The dissolution of AlCl₃ is exothermic. An ice bath is recommended. **Due to the separation difficulty of regioisomer products, *ortho*- and *para*-, in this step, the mixture was carried on to the next step and purification was achieved then. To a solution of biaryl ketone intermediate (250 mg, 0.73 mmol) in water (2 mL) was added conc. HCl (54 μ L, 0.63 mmol) at 0 °C, the resulting mixture was refluxed overnight. After completion of the reaction (monitored by LC/MS), 6M NaOH was added to neutralize the HCl (final pH ~8). The desired product was extracted with DCM, dried over Na₂SO₄, and concentrated under reduced pressure to yield an amber, viscous oil. Purification was performed on an automated flash chromatography system with 0-100% EtOAc in hexanes. The product elutes at ~40% EtOAc to afford **15** as a yellow solid (150 mg, 68%). R_f = 0.15 (20% EtOAc/hexanes); HPLC analysis (C18 reverse phase, 17 mins, 0-97% H₂O/ACN with 0.1% formic acid): **15** *para*- t_R = 10.4 min: **20** *ortho*- t_R = 10.7 min; ¹H NMR (400 MHz, 25 °C, CDCl₃): **15** *para*- δ 8.22 (1H, s), 8.07-8.00 (2H, m), 7.71 (2H, d, J = 8.6 Hz), 6.62 (2H, d, J = 8.6 Hz), 4.54 (1H, br), 2.96 (3H, d, J = 4.7 Hz); **20** *ortho*- δ 8.33 (1H, s), 8.15 (1H, d, J = 8.2 Hz), 8.02 (1H, d, J = 8.2 Hz), 7.32 (1H, t, J = 8.0 Hz), 7.03 (1H, s), 6.97 (1H, d, J = 7.4 Hz), 6.92-6.90 (1H, m), 4.00 (1H, br), 2.91 (3H, s); MS (ESI) m/z : [M + H]⁺ Calcd for C₁₄H₁₂N₃O₅ 302.1; Found **15** *para*- 302.3: **20** *ortho*- 302.4.

(3,4-Dinitrophenyl)(4-(methyl(oxetan-3-yl)amino)phenyl)methanol (16)

To a solution of **15** (500 mg, 1.66 mmol) in MeOH (8 mL) was added NaBH₄ (123 mg, 3.22 mmol). The resulting mixture was stirred at rt for 1 hr. Once the reaction was completed

(monitored by HPLC), the excess NaBH_4 was quenched by the addition of water, the product was extracted with DCM, dried over Na_2SO_4 , and concentrated under reduced pressure to yield an amber, viscous oil. Purification was performed on an automated flash chromatography system with 0-100% EtOAc in hexanes. The product elutes at ~40% EtOAc to afford **21** with a quantitative yield (503 mg). $R_f = 0.48$ (50% EtOAc/ hexanes); HPLC analysis (C18 reverse phase, 17 mins, 0-97% $\text{H}_2\text{O}/\text{ACN}$ with 0.1% formic acid): $t_R = 8.7$ min; ^1H NMR (400 MHz, 25°C , CDCl_3) δ 7.85 (1H, s), 7.77 (1H, d, $J = 8.3$ Hz), 7.61 (1H, d, $J = 8.8$ Hz), 7.00 (2H, d, $J = 8.3$ Hz), 6.49 (2H, d, $J = 8.3$ Hz), 5.66 (1H, s), 3.63 (1H, br), 2.73 (3H); MS (ESI) m/z : $[\text{M} + \text{H}]^+$ Calcd for $\text{C}_{14}\text{H}_{14}\text{N}_3\text{O}_5$ 304.1; Found 304.0. To a biaryl alcohol intermediate (6.25 g, 20.6 mmol) in MeOH (10 mL) was added oxetan-3-one (4 mL, 62.4 mmol) and acetic acid (2.4 mL, 41.2 mmol). The resulting mixture was stirred for 90 min at rt. Then $\text{NaBH}_3(\text{CN})$ (2.6 g, 41.4 mmol) was added and the reaction mixture was exposed to microwave irradiation for 3 hr at 65°C . Upon completion (monitored by LC/MS), the reaction was diluted with water, extracted with DCM, dried over Na_2SO_4 , and concentrated to yield an amber, viscous oil. Purification was performed on an automated flash chromatography system with 0-100% EtOAc in hexanes. The product elutes at ~55% EtOAc to afford **16** with 4.59 g (62%) yield. $R_f = 0.20$ (50% EtOAc/hexanes); HPLC analysis (C18 reverse phase, 17 mins, 0-97% $\text{H}_2\text{O}/\text{ACN}$ with 0.1% formic acid): $t_R = 9.8$ min; ^1H NMR (400 MHz, 25°C , CDCl_3) δ 7.94-7.89 (2H, m), 7.74 (1H, d, $J = 8.3$ Hz), 7.17 (2H, d, $J = 8.3$ Hz), 6.61 (2H, d, $J = 8.3$ Hz), 5.84 (1H, s), 4.87-4.84 (2H, m), 4.74-4.66 (3H, m), 2.94 (s, 3H); MS (ESI) m/z : $[\text{M} + \text{H}]^+$ Calcd for $\text{C}_{17}\text{H}_{18}\text{N}_3\text{O}_6$ 360.1; Found 360.1.

(3,4-Diaminophenyl)(4-(methyl(oxetan-3-yl)amino)phenyl)methanone (17)

Compound **16** (6.47 g, 18.0 mmol) was dissolved in DCM (90 mL) and Dess–Martin periodinane (15.3 g, 36.1 mmol) was added and the resulting mixture was stirred at rt for 1 hr. Upon completion (monitored by LC/MS), the reaction was diluted with water, extracted with DCM, dried over Na₂SO₄, and concentrated under reduced pressure to yield a dark yellow, viscous oil. Purification was performed on an automated flash chromatography system with 0-10% MeOH in DCM. The product elutes at ~4.5% MeOH to afford **22** with a 5.75 g (89%). *R*_f = 0.24 (50% EtOAc/hexanes); HPLC analysis (C18 reverse phase, 17 mins, 0-97% H₂O/ACN with 0.1% formic acid): *t*_R = 10.4 min; ¹H NMR (400 MHz, 25 °C, CDCl₃) δ 8.20 (1H, d, *J* = 1.2 Hz), 8.07-7.99 (2H, m), 7.72 (2H, d, *J* = 9.0 Hz), 6.65 (2H, d, *J* = 9.0 Hz), 5.04-4.98 (1H, m), 4.94 (2H, t, *J* = 6.8 Hz), 4.81 (2H, t, *J* = 6.5 Hz), 3.15 (s, 3H); MS (ESI) *m/z*: [M + H]⁺ Calcd for C₁₇H₁₆N₃O₆ 358.1; Found 358.1. To biaryl ketone intermediate (100 mg, 0.280 mmol) in MeOH (2 mL), Pd/C (10 wt % Pd/C, pre-wetted) was added and then a H₂-filled balloon attached to a 3-way valve was attached. The flask's atmosphere was repeatedly evacuated under vacuum and back-filled with H₂. The reaction was stirred for 24 hr then filtered through Celite, rinsing with additional MeOH. The solvent was removed under reduced pressure and the product was placed under high vacuum to yield **17** with dark orange, viscous oil (quantitative yield). *R*_f = 0.37 (10% MeOH/DCM); HPLC analysis (C18 reverse phase, 17 mins, 0-97% H₂O/ACN with 0.1% formic acid): *t*_R = 7.6 min; ¹H NMR (400 MHz, 25 °C, CDCl₃) δ 7.73 (2H, d, *J* = 8.8 Hz), 7.24 (1H, s), 7.20-7.18 (1H, m), 6.68 (1H, d, *J* = 7.8 Hz), 6.60 (2H, d, *J* = 8.8 Hz), 4.92-4.86 (3H, m), 4.80-4.79 (2H, m), 3.05 (3H, s); MS (ESI) *m/z*: [M + H]⁺ Calcd for C₁₇H₂₀N₃O₂ 298.2; Found 298.1.

Methyl (5-(4-(methyl(oxetan-3-yl)amino)benzoyl)-1H-benzo[d]imidazol-2-yl)carbamate (18)

Compound **17** (0.12 g, 0.44 mmol) was dissolved in MeOH (2 mL) and 1,3-bis(methoxycarbonyl)-2-methyl-2-thiopseudourea (0.18 g, 0.87 mmol) was added. The mixture was exposed to microwave irradiation (30 W) for 30 min for four times. Once the reaction was completed (monitored by LC/MS), the reaction mixture was concentrated under reduced pressure and residual oil was extracted with EtOAc and the organic phase washed with brine, dried with Na₂SO₄, and concentrated under reduced pressure to yield dark brown, viscous oil. Reversed phase purification was performed on an automated flash chromatography system. The product elutes at 18% MeCN in water with 0.1% formic acid to afford 0.114 g (68%) yield of a white amorphous solid. R_f = 0.53 (10% MeOH/DCM); HPLC analysis (C18 reverse phase, 17 mins, 0-97% H₂O/ACN with 0.1% formic acid): t_R = 8.3 min; ¹H NMR (400 MHz, 25 °C, CDCl₃) δ 10.76 (1H, br), 8.10 (1H, br), 7.82 (2H, d, J = 8.8 Hz), 7.77-7.63 (2H, m), 7.43 (1H, br), 6.65 (2H, d, J = 8.3 Hz), 4.95-4.93 (3H, m), 4.81 (2H, s), 3.87 (3H, s), 3.09 (3H, s); HRMS (ESI) m/z : [M + H]⁺ Calcd for C₂₀H₂₁N₄O₄ 381.1557; Found 381.1557.

Methyl (5-(2-(methyl(oxetan-3-yl)amino)benzoyl)-1H-benzo[d]imidazol-2-yl)carbamate (19)

Isolated by reversed phase purification on an automated flash chromatography system. The product elutes at 20% MeCN in water with 0.1% formic acid as a pale yellow solid; R_f = 0.38 (10% MeOH/DCM); HPLC analysis (C18 reverse phase, 17 mins, 0-97% H₂O/ACN with 0.1% formic acid): t_R = 8.4 min; ¹H NMR (400 MHz, 25 °C, CDCl₃) δ 7.82-7.69 (4H, m), 6.66-6.61 (3H, m), 4.93-4.81 (5H, m), 3.89 (3H, s), 3.10 (3H, s); MS (ESI) m/z : [M + H]⁺ Calcd for C₂₀H₂₁N₄O₄ 381.2; Found 381.3.

4.2. Solubility

4.2.1. Method development

A reverse phase HPLC/UV (Agilent 1200 with Thermo Scientific C18 column, particle size 2.6, dimensions 100 mm X 2.1 mm) method was applied as the analytical method for compound **18** and mebendazole. The compounds showed significant responses under 254 nm wavelength of the UV detector. The HPLC method was optimized by modification of mobile phase gradient (0 to 97% acetonitrile in water with 0.1% formic acid at a flow rate of 0.3 mL/min) and injection volume (5 μ L) to increase the sensitivity of compound under low concentration. Finally, a reverse phase HPLC with satisfying of limit of detection was developed for detecting compound **18** and mebendazole with concentration at 1 μ g/mL

4.2.2. Standard curve

Four levels of standard solutions of compound **18** and mebendazole were prepared using DMSO as dilution at 0.001, 0.01, 0.1, and 1 mg/mL. The linear equation between concentration and peak intensity was established and used to determine an analyte's concentration by comparison of the peak intensity versus known concentrations.

4.2.3. Sample preparation and analysis

Mebendazole (1 mg) or compounds **18** (1 mg) was initially dissolved in DMSO (8.4 μ L to each) and to each solution, PBS (phosphate buffer, pH 7.4, 159.6 μ L to each) was added to have the target concentration of 6.0 mg/mL with 5% DMSO. For kinetic study, the mixture was sonicated for 30 min at rt, centrifuged for 30 min (14,000 rpm). The supernatant (5 μ L) was analyzed by HPLC-UV, measured at 254 nm wavelength. For thermodynamic study, samples

from the sample preparation (6.0 mg/mL in PBS with 5% DMSO) were mixed by rotating 360 degree-wise at rt for 24 hr, centrifuged for 30 min (14,000 rpm), and the supernatant (5 μ L) was analyzed by HPLC-UV, measured at 254 nm wavelength. Aqueous concentration was determined by comparison of the peak intensity versus known concentrations.

4.3. Cell Culture

PC3, PC3MLN4, A549, Calu1, H157 (ATCC), and A549-TR cells were maintained in RPMI-1640, supplemented with 10% fetal bovine serum (FBS; Invitrogen) and 1% penicillin-streptomycin (P/S, Invitrogen). SKOV3 (ATCC) cells were maintained in McCoy's 5A (HyClone), 10% FBS, 1% P/S. All cell lines were kept at 37 °C with 5% CO₂.

4.4. Antibodies and Chemicals

Antibodies used in this work included the following: anti-Cyclin B1 (rabbit, Cell Signaling); anti-GAPDH HRP conjugated (Cell Signaling), monoclonal anti- α -tubulin (mouse, Sigma-Aldrich).

Mebendazole (Sigma-Aldrich) was reconstituted in DMSO (Sigma-Aldrich) to obtain 10 mM stock solutions. Aliquots were stored at -20 °C. Nocodazole (Sigma-Aldrich) was reconstituted in DMSO to obtain 20 mM stock solutions. Aliquots were stored at -20 °C. Compound **18** was reconstituted in DMSO to obtain 10 mM stock solutions. Aliquots were stored at -20 °C. Paclitaxel (#TXD01 by Cyoskeleton) was reconstituted in DMSO to obtain 2 mM stock solutions. Aliquots were stored at -20 °C.

4.5. Cell Viability Assays and EC_{50} determination

Cell survival assay using Cyquant reagent (Invitrogen, C7026) was performed following the manufacturer instructions. Briefly, 3×10^5 cells were seeded in 96-well plates overnight, before treatment with either vehicle or drug for 48 hr. Cells were harvested, washed and frozen at -80°C overnight. After thawing to room temperature, Cyquant reagent was added and fluorescence intensity was read with a spectrometer at 485 nm. Percent survival was calculated by dividing the reading from drug-treated cells by the reading from vehicle-treated cells. Median-dose effect analysis and EC_{50} calculation (50% reduction in cell survival) was performed using CompuSyn software (ComboSyn, Inc.).

MTT assay was performed in 96-well plates. First, 5×10^3 cells (PC3MLN4, A549, Calu1, H157, A549-TR) or 6×10^3 (PC3) or 8×10^3 (SKOV3) per well per 100 μL were seeded in 96-well plates. On the next day, 100 μL working stock of drug solution of **18** or mebendazole with 2X concentration of the final concentration was added to the cell suspension. After 72 hr drug incubation, 20 μL of 5 mg/mL MTT in PBS was added to the culture and incubated for 3.5 hr. Then, the media were removed and the precipitated was suspended in 1M HCl isopropanol. Absorbance was measured at 570 nm. Percent of cell viability was calculated by dividing the reading from drug-treated cells by the reading from vehicle-treated cells. EC_{50} calculation (50% reduction in cell viability) was performed using PrismGraph.

4.6. Immunofluorescent Staining and Microscopy

For immunofluorescent staining, cells were plated onto coverslips in 6-well plates, grown overnight and then treated with indicated drugs. After 48 hr of treatment, cells were washed with ice-cold PBS and fixed with 4% paraformaldehyde (PFA, Electron Microscopy Sciences) in PBS

for 15 min at rt. Cells were then permeabilized by incubation in 0.2% Triton X-100-PBS for 8 min. Next, cells were blocked with PBS blocking buffer containing 2% normal goat serum and 2% BSA for 1 hr at rt. Cells were incubated in an appropriated diluted primary antibody (1:200 anti- α -tubulin mouse antibody) for 1 hr at rt, washed with PBS and incubated in goat-anti-rabbit Alexa Fluor 488 (Molecular Probes) at 1:400 dilutions in blocking buffer for 45 min at rt. Finally, stained cells were washed with PBS, counterstained with 500 nM DAPI and mounted on slides with Prolong Gold antifade mounting media (Life Technologies).

4.7. Flow Cytometry Analysis and Cell Cycle Analysis

First, cells were seeded in 6-well plates (3×10^5 cell/well). On the next day, cells were treated for 24 hr with compound **18**, mebendazole, or nocodazole 1 μ M. The supernatant and the cell monolayer were collected, washed with PBS, and fixed with cold 70% ethanol for 30 min. Fixed cells were washed with PBS and incubated with PI (P-3566, Molecular Probes) and RNase A (Pure Link RNaseA, Invitrogen) for 30 min before FACS measurement. Measures were interrupted when 15×10^3 cells were counted for each sample. Data were analyzed with FlowJo software to fit the Dean-Jett Fox model.

4.8. Western Blot

Protein extracts were prepared using the lysis buffer (50 mM Tris, pH 7.5, 150 mM, NaCl, 10 mM NaF, and 0.5% NP40) freshly added with Proteinase Inhibitors Cocktail (Sigma Aldrich). Equal amounts of protein, as determined with a bicinchoninic acid (BCA) protein assay kit (Pierce/Thermo Scientific) used according to the manufacturer's instructions, were separated by SDS-PAGE and transferred to nitrocellulose membranes. The blots were blocked with 5% nonfat

dry milk in TBST (50 mM Tris-HCl, pH 7.4, 150 mM NaCl, and 0.1% Tween 20) and then incubated with appropriate primary antibodies. Signals were detected with horseradish peroxidase-conjugated secondary antibodies and enhanced chemiluminescence (ECL) detection system (Amersham/GE Healthcare).

4.9. *Mouse in vivo xenograft model*

All animal experiments were performed under guidelines approved by the Children's Hospital Boston Animal Care and Use Committee and Animal Resources Committee. Athymic eight-week-old male mice (Massachusetts General Hospital, MGH) were acclimated to a week prior to xenografting. PC3MNL4 cells (1×10^6) were resuspended in Growth Factor Reduced Matrigel (Corning) and Hank's Balanced Salt Solution (HBSS, 14175, Invitrogen) injected subcutaneously between the scapular of athymic mice using a 30-gauge needle. Tumor growth was measured with calipers, and drug treatment started 13 days after the cells injection, when tumor volume reached about 35 mm^3 . Mice were monitored three times per week for drug efficacy, as well for adverse effects, including weight and behavior. Drugs were administered by I.P. every other day, three times per week for two consecutive weeks. Mice were treated with compound **18** in 5% DMSO in HBSS 30 mg/kg; mebendazole in 5% DMSO in HBSS, 30 mg/kg; and 5% DMSO/HBSS for control group. Each testing group contained four to five mice (control $n = 5$; mebendazole 30 mg/kg, $n = 5$; compound **18** 30 mg/kg, $n = 4$). For calculating tumor volume, the following formula was used $Tumor\ volume = \frac{(tumor\ width)^2 \times tumor\ length}{2}$. The results were expressed as the mean (\pm SEM) of tumor volume in each group.

4.10. *Docking Study*

The two-dimensional structure and ionization state of compound **18** were drawn in two dimensions using MarvinDraw (Marvin 6.2.2, 2014, ChemAxon: <http://www.chemaxon.com>). The structure of compound **18** was converted into a low energy three-dimensional structure using Openbabel (v2.3.2) [54]. The tubulin crystal structure (PDB: 3HKC) and compound **18** were prepared for docking using Autodocktools (v1.5.6) [55]. Autodocking was performed using Autodock Vina (v1.1.2) and following the standard published docking protocol [48]. The low energy binding pose of compound **18** relative to tubulin was visualized using a combination of Autodocktools (v1.5.6) and UCSF chimera (v1.11) [55][56].

Competing interests

The authors declared no competing interests.

Author's contributions

JEC and YW synthesized the compounds. FEJ conducted the modeling study. MZ, IC, and YX carried out biological assays. JEC, MZ, BRZ, and LS drafted the manuscript. BRZ and LS conceived and directed the studies.

Acknowledgement

This research is partially supported by funding to BRZ from the David Koch Foundation and by seed funding for the Center for Drug Discovery and Translational Research at Beth Israel Deaconess Hospital (LS). We thank Dylan Frank for technical assistance. The Sponsors played no roles in study design, the collection, analysis and interpretation of data, the writing of the report, and the decision to submit the article for publication.

Appendix A. Supplementary material

Supplementary material related to this article can be found at

References

- [1] S.K. Pal, B. Lewis, O. Sartor, Management of docetaxel failures in metastatic castrate-resistant prostate cancer, *Urol. Clin. North Am.* 39 (2012) 583-591.
- [2] H. Beltran, T.M. Beer, M.A. Carducci, J. de Bono, M. Gleave, M. Hussain, W.K. Kelly, F. Saad, C. Sternberg, S.T. Tagawa, I.F. Tannock, New therapies for castration-resistant prostate cancer: efficacy and safety, *Eur. Urol.* 60 (2011) 279-290.
- [3] F. Saad, K. Miller, Treatment options in castration-resistant prostate cancer: current therapies and emerging docetaxel-based regimens, *Urol. Oncology*, 32 (2014) 70-79.
- [4] M.D. Balbas, M.J. Evans, D.J. Hosfield, J. Wongvipat, V.K. Arora, P.A. Watson, Y. Chen, G.L. Greene, Y. Shen, C.L. Sawyers, Overcoming mutation-based resistance to antiandrogens with rational drug design, *eLife*, 2 (2013) e00499.
- [5] J.M. Drake, N.A. Graham, J.K. Lee, T. Stoyanova, C.M. Faltermeier, S. Sud, B. Titz, J. Huang, K.J. Pienta, T.G. Graeber, O.N. Witte, Metastatic castration-resistant prostate cancer reveals inpatient similarity and interpatient heterogeneity of therapeutic kinase targets, *Proc. Natl. Acad. Sci. U.S.A.* 110 (2013) E4762-4769.
- [6] C.S. Grasso, Y.M. Wu, D.R. Robinson, X. Cao, S.M. Dhanasekaran, A.P. Khan, M.J. Quist, X. Jing, R.J. Lonigro, J.C. Brenner, I.A. Asangani, B. Ateeq, S.Y. Chun, J. Siddiqui, L. Sam, M. Anstett, R. Mehra, J.R. Prensner, N. Palanisamy, G.A. Ryslik, F. Vandin, B.J. Raphael, L.P. Kunju, D.R. Rhodes, K.J. Pienta, A.M. Chinnaiyan, S.A. Tomlins, The mutational landscape of lethal castration-resistant prostate cancer, *Nature*, 487 (2012) 239-243.
- [7] R.J. D'Amato, M.S. Loughnan, E. Flynn, J. Folkman, Thalidomide is an inhibitor of angiogenesis, *Proc. Natl. Acad. Sci. U.S.A.* 91 (1994) 4082-4085.

- [8] P.L. McCormack, Lenalidomide: a review of its continuous use in patients with newly diagnosed multiple myeloma not eligible for stem-cell transplantation, *Drugs & Aging*, 32 (2015) 409-418.
- [9] V. Hanusova, L. Skalova, V. Kralova, P. Matouskova, Potential anti-cancer drugs commonly used for other indications, *Curr. Cancer Drug Targets*, 15 (2015) 35-52.
- [10] B.T. Aftab, I. Dobromilskaya, J.O. Liu, C.M. Rudin, Itraconazole inhibits angiogenesis and tumor growth in non-small cell lung cancer, *Cancer Res.* 71 (2011) 6764-6772.
- [11] J. Kim, J.Y. Tang, R. Gong, J. Kim, J.J. Lee, K.V. Clemons, C.R. Chong, K.S. Chang, M. Fereshteh, D. Gardner, T. Reya, J.O. Liu, E.H. Epstein, D.A. Stevens, P.A. Beachy, Itraconazole, a commonly used antifungal that inhibits Hedgehog pathway activity and cancer growth, *Cancer Cell*, 17 (2010) 388-399.
- [12] R. Liu, J. Li, T. Zhang, L. Zou, Y. Chen, K. Wang, Y. Lei, K. Yuan, Y. Li, J. Lan, L. Cheng, N. Xie, R. Xiang, E.C. Nice, C. Huang, Y. Wei, Itraconazole suppresses the growth of glioblastoma through induction of autophagy: involvement of abnormal cholesterol trafficking, *Autophagy*, 10 (2014) 1241-1255.
- [13] Z.J. Hou, X. Luo, W. Zhang, F. Peng, B. Cui, S.J. Wu, F.M. Zheng, J. Xu, L.Z. Xu, Z.J. Long, X.T. Wang, G.H. Li, X.Y. Wan, Y.L. Yang, Q. Liu, Flubendazole, FDA-approved anthelmintic, targets breast cancer stem-like cells, *Oncotarget*, 6 (2015) 6326-6340.
- [14] V. Kralova, V. Hanusova, E. Rudolf, K. Canova, L. Skalova, Flubendazole induces mitotic catastrophe and senescence in colon cancer cells in vitro, *J. Pharmacy and Pharmacol.* 68 (2016) 208-218.
- [15] M. Michaelis, B. Agha, F. Rothweiler, N. Loschmann, Y. Voges, M. Mittelbronn, T. Starzetz, P.N. Harter, B.A. Abhari, S. Fulda, F. Westermann, K. Riecken, S. Spek, K. Langer, M.

Wiese, W.G. Dirks, R. Zehner, J. Cinatl, M.N. Wass, J. Cinatl, Jr., Identification of flubendazole as potential anti-neuroblastoma compound in a large cell line screen, *Sci. Rep.* 5 (2015) 8202.

[16] P.A. Spagnuolo, J. Hu, R. Hurren, X. Wang, M. Gronda, M.A. Sukhai, A. Di Meo, J. Boss, I. Ashali, R. Beheshti Zavareh, N. Fine, C.D. Simpson, S. Sharmeen, R. Rottapel, A.D. Schimmer, The antihelmintic flubendazole inhibits microtubule function through a mechanism distinct from Vinca alkaloids and displays preclinical activity in leukemia and myeloma, *Blood*, 115 (2010) 4824-4833.

[17] I. Bodhinayake, M. Symons, J.A. Boockvar, Repurposing mebendazole for the treatment of medulloblastoma, *Neurosurg.* 76 (2015) N15-16.

[18] M. De Witt, A. Gamble, D. Hanson, D. Markowitz, C. Powell, S. Al Dimassi, M. Atlas, J. Boockvar, R. Ruggieri, M. Symons, Repurposing mebendazole as a replacement for vincristine for the treatment of brain tumors, *Mol. Med.* 23 (2017) 50-56.

[19] A.R. Larsen, R.Y. Bai, J.H. Chung, A. Borodovsky, C.M. Rudin, G.J. Riggins, F. Bunz, Repurposing the antihelmintic mebendazole as a hedgehog inhibitor, *Mol. Cancer Ther.* 14 (2015) 3-13.

[20] D. Martarelli, P. Pompei, C. Baldi, G. Mazzoni, Mebendazole inhibits growth of human adrenocortical carcinoma cell lines implanted in nude mice, *Cancer Chemother. Pharmacol.* 61 (2008) 809-817.

[21] T. Mukhopadhyay, J. Sasaki, R. Ramesh, J.A. Roth, Mebendazole elicits a potent antitumor effect on human cancer cell lines both in vitro and in vivo, *Clin. Cancer Res.* 8 (2002) 2963-2969.

[22] C.A. Pettaway, S. Pathak, G. Greene, E. Ramirez, M.R. Wilson, J.J. Killian, I.J. Fidler, Selection of highly metastatic variants of different human prostatic carcinomas using orthotopic implantation in nude mice, *Clin. Cancer Res.* 2 (1996) 1627-1636.

- [23] S. Marchiani, L. Tamburrino, G. Nesi, M. Paglierani, S. Gelmini, C. Orlando, M. Maggi, G. Forti, E. Baldi, Androgen-responsive and -unresponsive prostate cancer cell lines respond differently to stimuli inducing neuroendocrine differentiation, *Int. J. Andrology*, 33 (2010) 784-793.
- [24] S. Tai, Y. Sun, J.M. Squires, H. Zhang, W.K. Oh, C.Z. Liang, J. Huang, PC3 is a cell line characteristic of prostatic small cell carcinoma, *The Prostate*, 71 (2011) 1668-1679.
- [25] L.J. Jones, M. Gray, S.T. Yue, R.P. Haugland, V.L. Singer, Sensitive determination of cell number using the CyQUANT cell proliferation assay, *J. Immunol. Methods*, 254 (2001) 85-98.
- [26] K. Canova, L. Rozkydalova, E. Rudolf, Anthelmintic Flubendazole and Its Potential Use in Anticancer Therapy, *Acta Medica (Hradec Kralove)*, 60 (2017) 5-11.
- [27] I. Shehatta, Cyclodextrins as enhancers of the aqueous solubility of the anthelmintic drug mebendazole: thermodynamic considerations, *Monatsh. Chem.* 133 (2002) 1239-1247.
- [28] Y. Chiba, N. Kohri, K. Iseki, K. Miyazaki, Improvement of dissolution and bioavailability for mebendazole, an agent for human echinococcosis, by preparing solid dispersion with polyethylene glycol, *Chem. Pharm. Bull.* 39 (1991) 2158-2160.
- [29] J.D. Baggot, Q.A. McKellar, The absorption, distribution and elimination of anthelmintic drugs: the role of pharmacokinetics, *J. Vet. Pharmacol. Ther.* 17 (1994) 409-419.
- [30] M. Michiels, R. Hendriks, J. Heykants, H. van den Bossche, The pharmacokinetics of mebendazole and flubendazole in animals and man, *Arch. Int. Pharmacodyn. Ther.* 256 (1982) 180-191.
- [31] L. Di, P.V. Fish, T. Mano, Bridging solubility between drug discovery and development, *Drug Discov. Today*, 17 (2012) 486-495.
- [32] M.J. Waring, J. Arrowsmith, A.R. Leach, P.D. Leeson, S. Mandrell, R.M. Owen, G. Pairaudeau, W.D. Pennie, S.D. Pickett, J. Wang, O. Wallace, A. Weir, An analysis of the

attrition of drug candidates from four major pharmaceutical companies, *Nat. Rev. Drug. Discov.* 14 (2015) 475-486.

[33] G. Wuitschik, E.M. Carreira, B. Wagner, H. Fischer, I. Parrilla, F. Schuler, M. Rogers-Evans, K. Muller, Oxetanes in drug discovery: structural and synthetic insights, *J. Med. Chem.* 53 (2010) 3227-3246.

[34] J.A. Burkhard, G. Wuitschik, M. Rogers-Evans, K. Muller, E.M. Carreira, Oxetanes as versatile elements in drug discovery and synthesis, *Angew. Chem. Int. Ed.* 49 (2010) 9052-9067.

[35] S. Wagaw, S.L. Buchwald, The synthesis of aminopyridines: a method employing palladium-catalyzed carbon-nitrogen bond formation, *J. Org. Chem.* 61 (1996) 7240-7241.

[36] H. Park, S. Hong, J. Kim, S. Hong, Discovery of picomolar ABL kinase inhibitors equipotent for wild type and T315I mutant via structure-based de novo design, *J. Am. Chem. Soc.* 135 (2013) 8227-8237.

[37] D.B. Dess, J.C. Martin, A useful 12-I-5 triacetoxypersulfonane (the Dess-Martin persulfonane) for the selective oxidation of primary or secondary alcohols and a variety of related 12-I-5 species, *J. Am. Chem. Soc.* 113 (1991) 7277-7287.

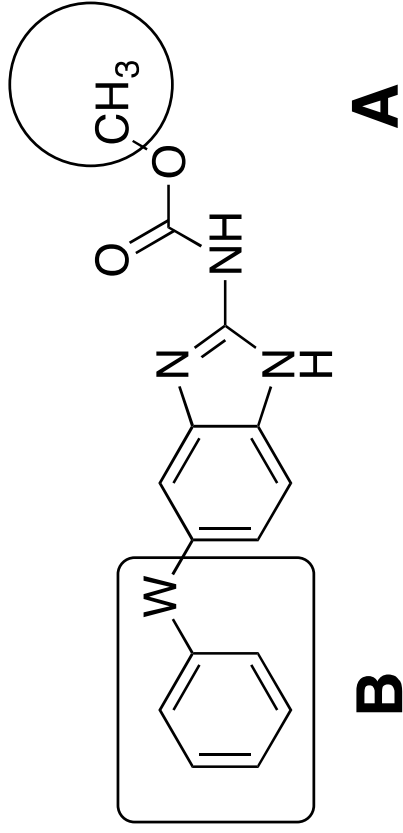
[38] N. Patel, S.K. Chatterjee, V. Vrbancic, I. Chung, C.J. Mu, R.R. Olsen, C. Waghorne, B.R. Zetter, Rescue of paclitaxel sensitivity by repression of Prohibitin1 in drug-resistant cancer cells, *Proc. Natl. Acad. Sci. U. S. A.* 107 (2010) 2503-2508.

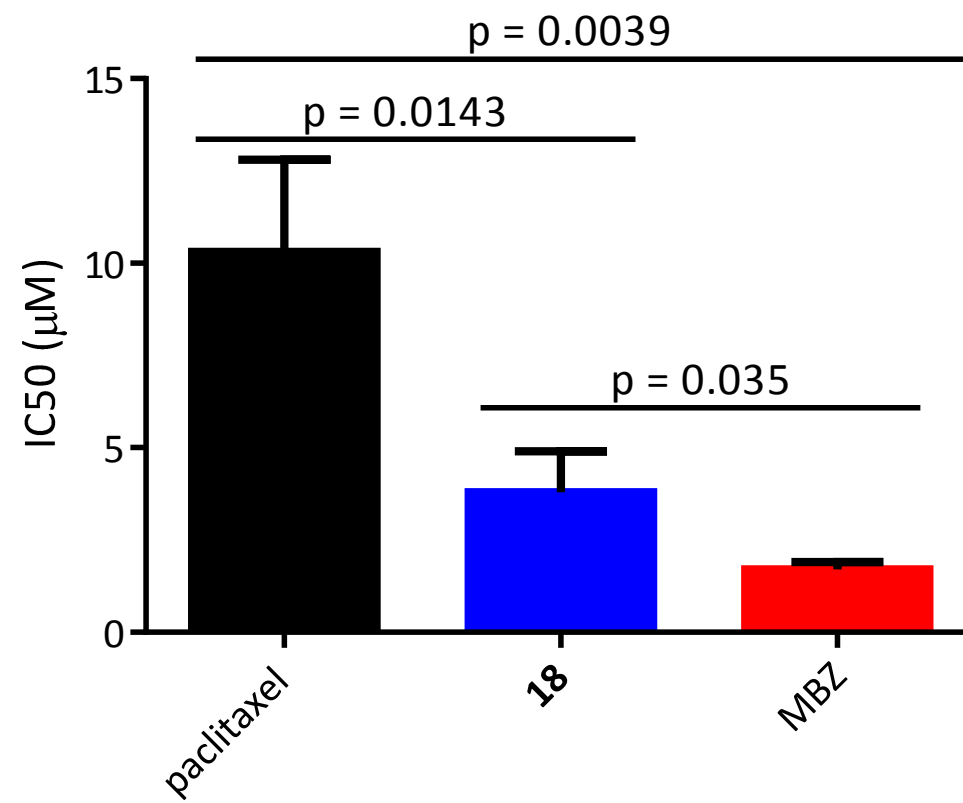
[39] G.W. Zieve, D. Turnbull, J.M. Mullins, J.R. McIntosh, Production of large numbers of mitotic mammalian cells by use of the reversible microtubule inhibitor Nocodazole, *Exp. Cell Res.* 126 (1980) 397-405.

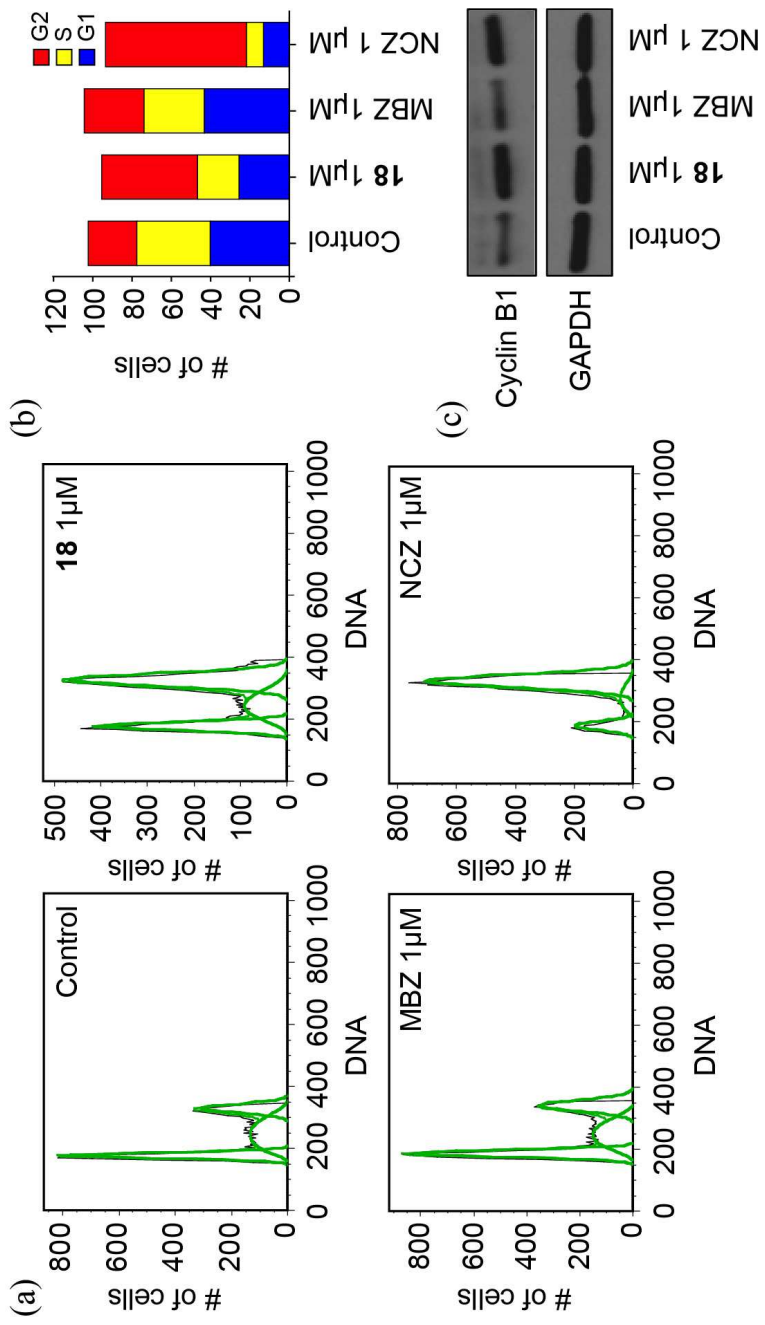
[40] M.H. Fox, A model for the computer analysis of synchronous DNA distributions obtained by flow cytometry, *Cytometry*, 1 (1980) 71-77.

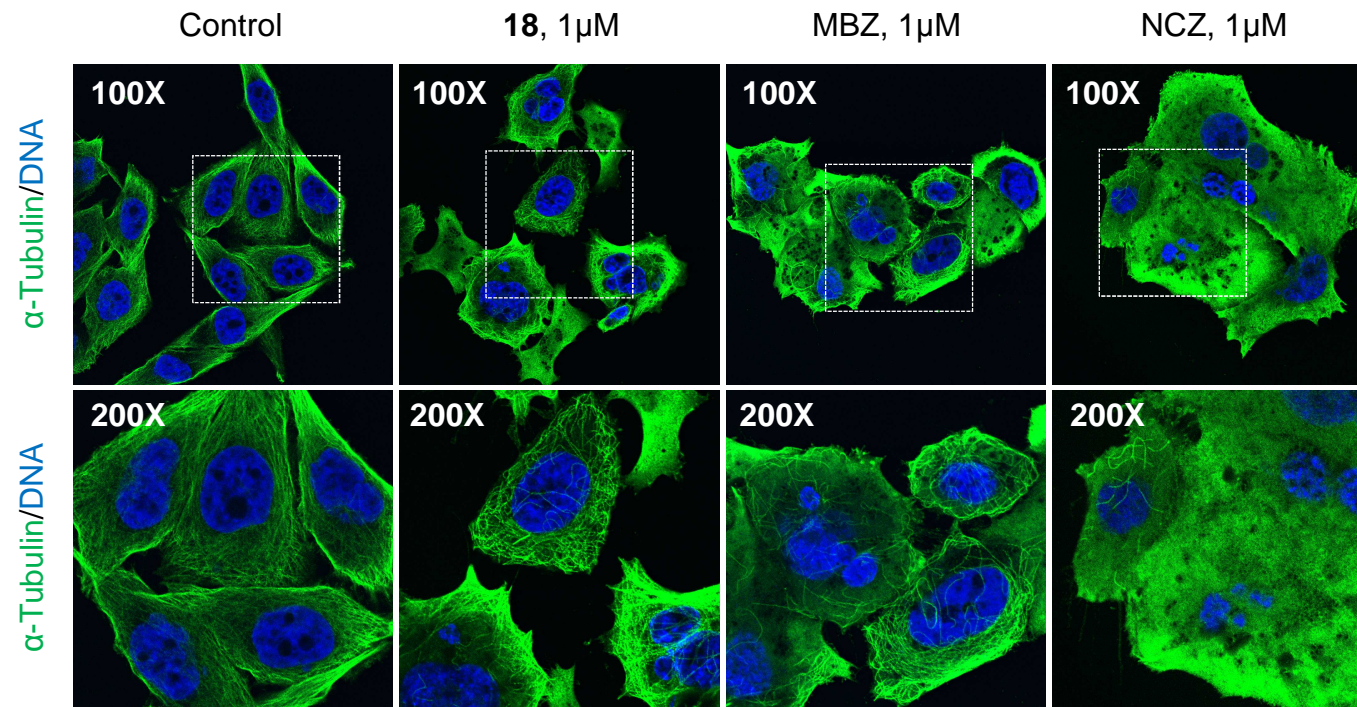
- [41] C.M. Ireland, K. Gull, W.E. Gutteridge, C.I. Pogson, The interaction of benzimidazole carbamates with mammalian microtubule protein, *Biochem. Pharmacol.* 28 (1979) 2680-2682.
- [42] J.P. Laclette, G. Guerra, C. Zetina, Inhibition of tubulin polymerization by mebendazole, *Biochem. Biophys. Res. Commun.* 92 (1980) 417-423.
- [43] P.A. Friedman, E.G. Platzer, Interaction of anthelmintic benzimidazoles with *Ascaris suum* embryonic tubulin, *Biochim. Biophys. Acta*, 630 (1980) 271-278.
- [44] N.A. Doudican, S.A. Byron, P.M. Pollock, S.J. Orlow, XIAP downregulation accompanies mebendazole growth inhibition in melanoma xenografts, *Anticancer Drugs*, 24 (2013) 181-188.
- [45] K.L. Cheng, T. Bradley, D.R. Budman, Novel microtubule-targeting agents - the epothilones, *Biologics*, 2 (2008) 789-811.
- [46] N.F. Dybdal-Hargreaves, A.L. Risinger, S.L. Mooberry, Eribulin mesylate: mechanism of action of a unique microtubule-targeting agent, *Clin. Cancer Res.* 21 (2015) 2445-2452.
- [47] Y.F. Wang, Q.W. Shi, M. Dong, H. Kiyota, Y.C. Gu, B. Cong, Natural taxanes: developments since 1828, *Chem. Rev.* 111 (2011) 7652-7709.
- [48] O. Trott, A.J. Olson, AutoDock Vina: improving the speed and accuracy of docking with a new scoring function, efficient optimization, and multithreading, *J. Comput. Chem.* 31 (2010) 455-461.
- [49] A. Dorleans, B. Gigant, R.B. Ravelli, P. Mailliet, V. Mikol, M. Knossow, Variations in the colchicine-binding domain provide insight into the structural switch of tubulin, *Proc. Natl. Acad. Sci. U. S. A.* 106 (2009) 13775-13779.
- [50] K. Sugano, A. Okazaki, S. Sugimoto, S. Tavornvipas, A. Omura, T. Mano, Solubility and dissolution profile assessment in drug discovery, *Drug Metab. Pharmacokinet.* 22 (2007) 225-254.

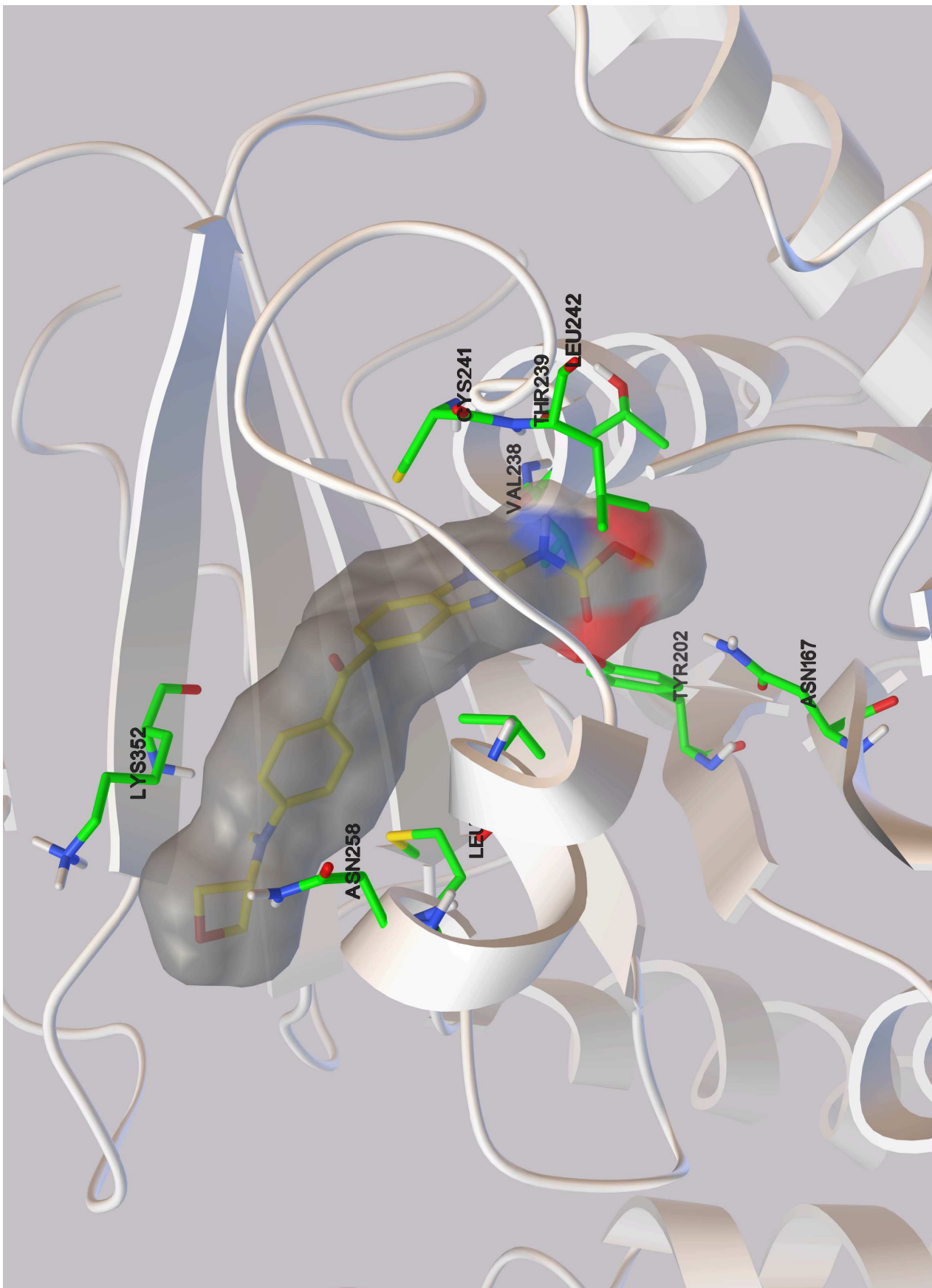
- [51] C.A. Lipinski, Drug-like properties and the causes of poor solubility and poor permeability, *Journal of pharmacological and toxicological methods*, 44 (2000) 235-249.
- [52] H.D. Williams, N.L. Trevaskis, S.A. Charman, R.M. Shanker, W.N. Charman, C.W. Pouton, C.J. Porter, Strategies to address low drug solubility in discovery and development, *Pharmacological reviews*, 65 (2013) 315-499.
- [53] J. Wu, Statistical inference for tumor growth inhibition T/C ratio, *J Biopharm Stat*, 20 (2010) 954-964.
- [54] N.M. O'Boyle, M. Banck, C.A. James, C. Morley, T. Vandermeersch, G.R. Hutchison, Open Babel: An open chemical toolbox, *J Cheminform*, 3 (2011) 33.
- [55] G.M. Morris, R. Huey, W. Lindstrom, M.F. Sanner, R.K. Belew, D.S. Goodsell, A.J. Olson, AutoDock4 and AutoDockTools4: Automated docking with selective receptor flexibility, *J Comput Chem*, 30 (2009) 2785-2791.
- [56] E.F. Pettersen, T.D. Goddard, C.C. Huang, G.S. Couch, D.M. Greenblatt, E.C. Meng, T.E. Ferrin, UCSF Chimera-a visualization system for exploratory research and analysis, *J Comput Chem*, 25 (2004) 1605-1612.



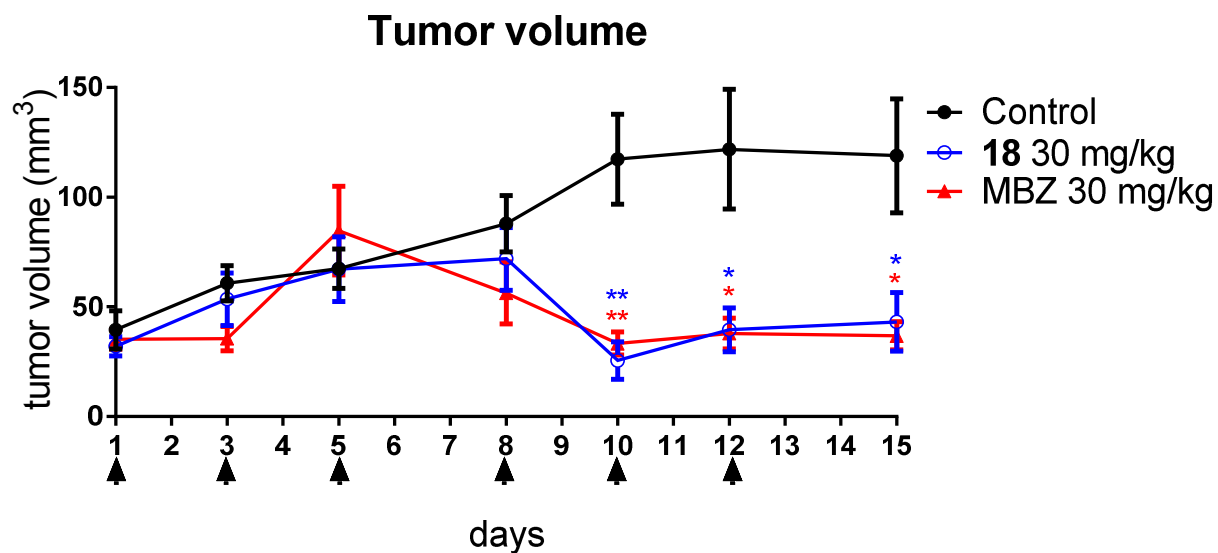




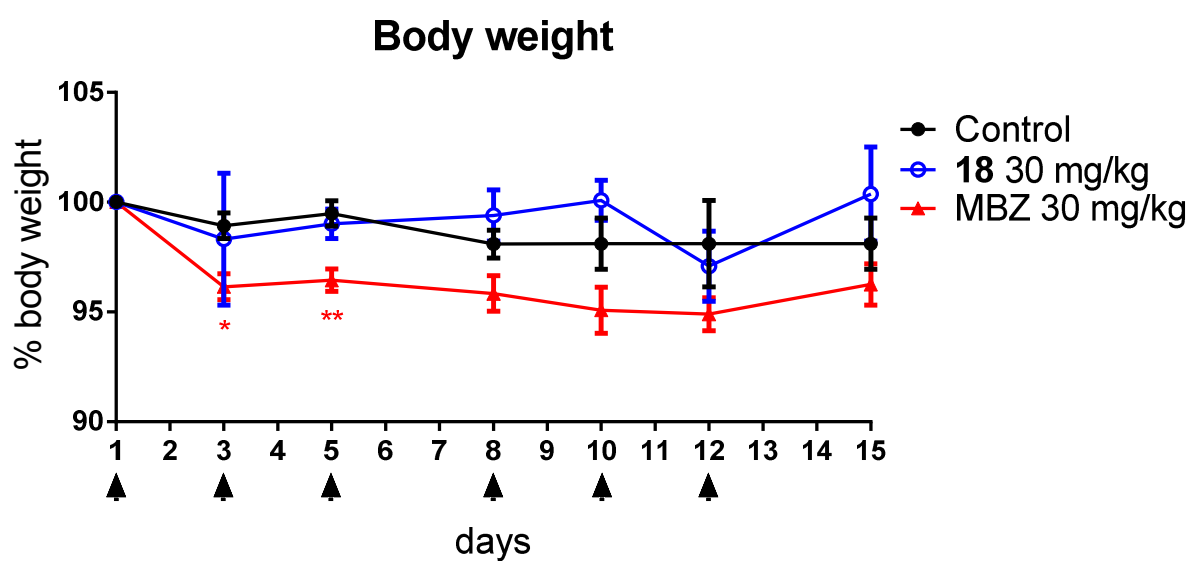




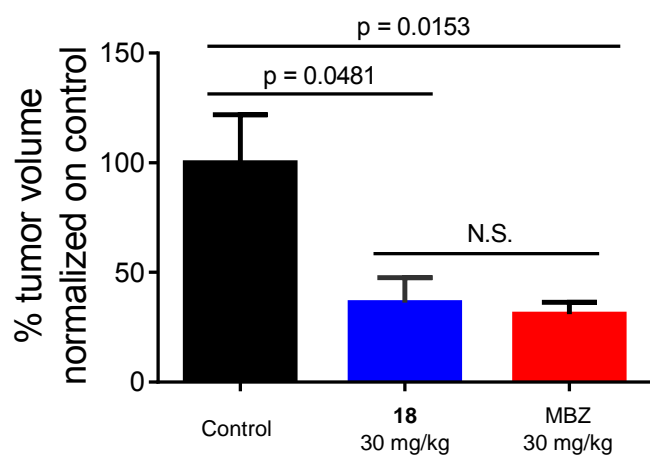
(a)



(b)



(c)



Highlights

- SAR study led to the discovery of the novel oxetane-containing benzimidazole methylcarbamate (Compound **18**) as an anticancer drug lead.
- Compound **18** showed drastically increased aqueous solubility (361 μM) and potent cytotoxicity in prostate, lung, and ovarian cancer cell lines (IC_{50} : 0.9-3.8 μM).
- At 30mg/kg, Compound **18** inhibited tumor growth (T/C: 0.36) in a mouse xenograft model of the highly aggressive PC3MLN4 prostate cancer.